Atmos. Chem. Phys. Discuss., doi:10.5194/acp-2016-656, 2016
Manuscript under review for journal Atmos. Chem. Phys.
Published: 19 September 2016

Atmospheric Chemistry and Physics
Discussions

Probing the subtropical lowermost stratosphere, tropical upper troposphere, and tropopause layer for inorganic bromine

B. Werner[1], J. Stutz[2], M. Spolaor[2], L. Scalone[1], R. Raecke[1], J. Festa[2], F. Colosimo[2], R. Cheung[2], C. Tsai[2], R. Hossaini[3], M. P. Chipperfield[4], G. S. Taverna[4], W. Feng[5], J. W. Elkins[6], D. W. Fahey[6], Ru-Shan Gao[6], E. J. Hintsa[6,7], T. D. Thornberry[6,7], F. L. Moore[6,7], M. A. Navarro[8], E. Atlas[8], B. Daube[9], J. Pittman[9], S. Wofsy[9], and K. Pfeilsticker[1]

[1]Institute of Environmental Physics, University of Heidelberg, Heidelberg, Germany
[2]Department of Atmospheric and Oceanic Science, University of California Los Angeles, Los Angeles, California, USA
[3]Lancaster Environment Centre, University of Lancaster, Lancaster, UK
[4]Institute for Climate and Atmospheric Science, School of Earth and Environment, University of Leeds, Leeds, UK
[5]National Centre for Atmospheric Science, School of Earth and Environment, University of Leeds, UK
[6]NOAA Earth System Research Laboratory, Boulder, Colorado, USA
[7]Cooperative Institute for the Research in the Environmental Sciences (CIRES), University of Colorado, Boulder, Colorado, USA
[8]The Rosenstiel School of Marine and Atmospheric Science, University of Miami, Miami, Florida, USA
[9]School of Engineering and Applied Sciences, Harvard University, Cambridge, Massachusetts, USA

Correspondence to: Klaus Pfeilsticker
(Klaus.Pfeilsticker@iup.uni-heidelberg.de)

Abstract. We report on measurements of CH_4, O_3, NO_2, BrO and some key brominated source gases within the subtropical lowermost stratosphere (LS), tropical upper troposphere (UT) and tropopause layer (TTL) (14 - 18.5 km). The measurements were performed within the framework of the NASA-ATTREX (National Aeronautics and Space Administration - Airborne Tropical Tropopause Experiment) project from aboard the Global Hawk (GH) during 6 deployments over the Eastern Pacific in early 2013. O_3, NO_2, and BrO were remotely monitored by analyzing limb scattered skylight in the UV and visible spectral ranges using the observations of the mini-DOAS (Differential Optical Absorption Spectroscopy) instrument (Stutz et al., 2016). CH_4 was measured in-situ by the Harvard HUPCRS instrument and by the NOAA-UCATS instrument. O_3 was recorded at high precision by the NOAA dual-beam UV photometer, and some key brominated source gases were analyzed in whole air samples of the GWAS (Global Hawk Whole Air Sampler) instrument. All of these measurements are used for comparison with TOMCAT/SLIMCAT 3-D model simulations, aiming at improvements of our understanding of the bromine budget and photochemistry in the LS, UT, and TTL.

Potential changes in local O_3 (and NO_2 and BrO) due to transport processes are separated from photochemical processes in inter-comparisons of measured and modeled CH_4 and O_3. After accounting for some minor deficiencies in the details of the modeled vertical transport, excellent agreement is achieved among measured and simulated CH_4 and O_3, indicating that in the subtropical LS and TTL O_3 concentrations mostly vary due to dynamical rather than photochemical processes. The TOMCAT/SLIMCAT simulations are further used for the interpretation of the measured NO_2 and BrO. In excellent agreement with the model predictions, NO_2 concentrations are found to range between 70 - 170 ppt in the subtropical LS, and in the TTL they are close to, or below the detection limit of 15 ppt in daytime. The measured BrO concentrations range between 3 - 9 ppt in the subtropical LS, and in the TTL they reach 0.5 ± 0.5 ppt at the bottom of the TTL (150 hPa/355 K/14 km) and up to about 5 ppt at the top of the TTL (70 hPa/425 K/18.5 km, for the TTL definition see Fueglistaler et al. (2009)), in overall good agreement with the model simulation, and the expectation based on the destruction of brominated source gases.

The TOMCAT/SLIMCAT simulations tend to slightly under-predict measured BrO depending on the photochemical regime studied, even when constrained to the measured $\mathrm{O_3}$ and $\mathrm{NO_2}$, and adjusted to match the observed concentrations of some key brominated source gases. The measured BrO and modeled $\mathrm{BrO/Br_y^{inorg}}$ ratio is further used to calculate inorganic bromine, $\mathrm{Br_y^{inorg}}$. For the TTL (i.e. when $[\mathrm{CH_4}] \geq$ 1390 ppb), $\mathrm{Br_y^{inorg}}$ is found to increase from a mean of 2.63 ± 1.04 ppt for θ in the range of 350 - 360 K to 5.11 ± 1.57 ppt for $\theta = 390 - 400$ K, whereas in the subtropical LS (i.e. when $[\mathrm{CH_4}] \leq$ 1390 ppb), it reaches 7.66 ± 2.95 ppt for θ in the range of 390 - 400 K. Finally, the TOMCAT/SLIMCAT simulations indicate a net destruction of ozone of - 0.5 ppbv/day at the base of the TTL (θ = 355 K) and a net production of + 1.8 ppbv/day at its top (θ = 383 K).

1 Introduction

At present bromine is estimated to be responsible for roughly 1/3 of the observed global chemical depletion in stratospheric ozone (WMO, 2014). Past research has revealed that total stratospheric bromine ($\mathrm{Br_y}$) has (in 2013) 4 major sources, or contributions: (1) $\mathrm{CH_3Br}$ which is mostly emitted by natural and anthropogenic sources with a present contribution of 6.9 ppt to $\mathrm{Br_y}$, (2) 4 major halons ($\mathrm{CClBrF_2}$ or Halon-1211; $\mathrm{CBrF_3}$ or Halon-1301; $\mathrm{CBr_2F_2}$ or halon-1202 and $\mathrm{CBrF_2CBrF_2}$ or halon-2402) all emitted from anthropogenic activities with a present contribution of 8 ppt to $\mathrm{Br_y}$, and (3) so-called very short-lived species (VSLS), and (4) inorganic bromine of the upper troposphere which is transported into the stratosphere. Together sources 3 and 4 are assessed to contribute 5 (2 - 8) ppt to stratospheric bromine (WMO, 2014). Previous assessments of total $\mathrm{Br_y}$ and its trend revealed $[\mathrm{Br_y}]$ levels of ≈ 20 ppt (16 - 23 ppt) in 2011, which has been decreasing at a rate of -0.6 $\%/\mathrm{yr}$ since the peak levels observed in 2000. This decline is consistent with the decrease in total organic bromine in the troposphere based on measurements of $\mathrm{CH_3Br}$, and the halons (WMO, 2014).

Estimates of stratospheric $\mathrm{Br_y}$ essentially rely on two methods: First, the so-called organic ($\mathrm{Br_y^{org}}$) method, where all bromine from organic source gases (SG) found at stratospheric entry level is summed (Wamsley et al. (1998), Pfeilsticker et al. (2000), Sturges et al. (2000), Brinckmann et al. (2012), Navarro et al. (2015)). Second, total inorganic bromine ($\mathrm{Br_y^{inorg}}$) is inferred from atmospheric measurements (e.g., performed from the ground, aircraft, high-flying balloons, or satellites) of the most abundant $\mathrm{Br_y}$ species, BrO, assisted by a suitable correction for the $\mathrm{Br_y^{inorg}}$ partitioning inferred from photochemical modeling (e.g., Pfeilsticker et al. (2000), Richter et al. (2002), Van Roozendael et al. (2002), Sioris et al. (2006), Dorf et al. (2006a), Hendrick et al. (2007), Dorf et al. (2008), Theys et al. (2009), Theys et al. (2011), Rozanov et al. (2011), Parrella et al. (2013), Stachnik et al. (2013), and others). While the organic method is rather precise for the measured species (accuracies are several 0.1 ppt), it suffers from the shortcoming of not accounting for any inorganic bromine (contribution 4) directly entering the stratosphere. Uncertainties in the inorganic method arise from uncertainties in measuring BrO as well as from modeling

Br_y^{inorg} partitioning, of which the combined error amounts to $\pm(2.5-4)$ ppt, depending on the type of observation and probed photochemical regime.

Past in-situ measurements of Br_y^{org} were performed at different locations and seasons within the upper troposphere, TTL, and stratosphere. In the present context the most important were measurements performed within the TTL (for the TTL definition see Fueglistaler et al. (2009)) over the Pacific from where most of the stratospheric air is predicted to originate (e.g., Fueglistaler et al. (2009), Aschmann et al. (2009), Hossaini et al. (2012b), Ashfold et al. (2012), WMO (2014), Orbe et al. (2015), and others). These include the measurements (a) by Schauffler et al. (1993), Schauffler et al. (1998), and Schauffler et al. (1999), who found [VSLS] = 1.3 ppt (contribution 3) at the tropical tropopause over the central Pacific (Hawaii) in 1996, (b) by Laube et al. (2008), and Brinckmann et al. (2012) with [VSLS] = 2.25 ± 0.24 ppt (range 1.4 - 4.6 ppt) and [VSLS] = 1.35 ppt (range 0.7 - 3.4 ppt) found within the TTL over north eastern Brazil in June 2005 and June 2008, respectively, and (c) most recently those by Navarro et al. (2015), who found [VSLS] = 2.96±0.42 ppt and 3.27±0.49 ppt at 17 km over the tropical Eastern and Western Pacific in 2013, and 2014, respectively. Information on contribution 3 was further corroborated by measurements performed in the upper tropical troposphere by (b) Sala et al. (2014) who found [VSLS] = 3.72 ± 0.60 ppt in the upper tropical troposphere over Borneo in fall 2011 and (c) by Wisher et al. (2014), who inferred [VSLS] = 3.4 ± 1.5 ppt for the CARIBIC flights from Germany to Venezuela/Columbia during 2009 - 2011, Germany to South Africa during 2010 and 2011, and Germany to Thailand/Kuala Lumpur, Malaysia during 2012 and 2013, and others.

Supporting information on brominated VSLS concentrations typical for the boundary layer of the Western Pacific came from measurements performed during the TransBrom ship cruise in October 2009 (median 2.23 ppt and range from 1.45 - 4.14 ppt, Brinckmann et al. (2012)) and the VSLS measurements made during the SHIVA project (median 5.7 ppt and range from 3.9 - 10.7 ppt, Sala et al. (2014)). Corroborating model calculations to these field studies by (a) Tegtmeier et al. (2012) indicated that from the Western Pacific on average only 0.4 ppt and at maximum up to 2.3 ppt of the emitted VSLS bromine may reach the stratosphere, while (b) Liang et al. (2014) estimated that up to 8 ppt of VSLS bromine may enter the base of the TTL at 150 hPa, whereby the VSLS emissions from the tropical Indian Ocean, the tropical western Pacific, and off the Pacific coast of Mexico are suspected to be most relevant, and finally (c) the CAM-Chem modeling performed within the study of Navarro et al. (2015) which indicates that over the Eastern and Western Pacific contributions 3 and 4 (called [VSLS + Br_y^{inorg}] in the study) amount to 6.20 (range 3.79 - 8.61) ppt and 5.81 (range 5.14 -6.48) ppt, respectively.

Using the inorganic method contributions 3 and 4 have been indirectly estimated from measured BrO performed at the ground, high flying balloons, or satellites (e.g., Pfeilsticker et al. (2000), Richter et al. (2002), Van Roozendael et al. (2002), Sioris et al. (2006), Dorf et al. (2006b), Hendrick et al. (2007), Dorf et al. (2008), Theys et al. (2009), Theys et al. (2011), Rozanov et al. (2011), Parrella et al. (2013), Stachnik et al. (2013), and others). All together these studies pointed to a range between 3 - 8 ppt with a mean of 6 ppt for contributions 3 and 4. The most direct information on contribution 3 and 4 came by the study of Dorf et al. (2008), who inferred 4.0 ± 2.5 ppt and 2.5 ± 2.6 ppt for contribution 3 and 4 from two balloon-borne soundings performed in the TTL and stratosphere over north-eastern Brazil during the dry season in 2005, and 2008, respectively. The inferred bromine was thus often larger than [VSLS] inferred using the organic method (contribution

3), indicating that eventually some Br_y^{inorg} (i.e. several ppt) is directly transported from the troposphere into the stratosphere (contribution 4).

Based on these findings, Hossaini et al. (2015) provided evidence for the efficiency of short-lived halogens to influence climate through depletion of lower stratospheric ozone (for contribution 3), but without explicitly considering the effect of inorganic bromine readily transported across the tropical tropopause (i.e. contribution 4). They concluded that VSLS bromine alone exerts a 3.6 times larger ozone radiative effect than due to long-lived halocarbons, when normalized to their halogen content. Moreover the benefit for ozone and UV radiation due to the declining stratospheric chlorine and bromine since the implementation of the Montreal protocol was quantified in a recent study by Chipperfield et al. (2015).

The present paper reports on measurements of BrO (and NO_2, O_3, CH_4, and the brominated source gases) made during the ATTREX deployments of the NASA Global Hawk into the LS, UT, and TTL of the Eastern Pacific in early 2013. Corresponding data collected during the Western Pacific deployments in early 2014 will be reported in a forthcoming paper, primarily since most of the 2014 measurements were performed under TTL cirrus-affected conditions, for which the interpretation of UV/vis spectroscopic measurements is not straightforward (see below). The present paper further addresses the amount of inorganic bromine found in the TTL, and its transport into the lowermost tropical stratosphere (contribution 4), together with the implications for ozone.

Our study accompanies those of Navarro et al. (2015) and Stutz et al. (2016). While Stutz et al. (2016) discusses the instrumental details and the methods employed to remotely measure BrO, NO_2, and O_3, the study of Navarro et al. (2015) reports on the GWAS measurements of CH_3Br (contribution 1), the halons (contribution 2), and the brominated VSLS (contribution 3) analyzed in whole air samples, which were simultaneously taken from aboard the NASA Global Hawk over the Eastern and Western Pacific during the 2013 and 2014 deployments, respectively.

The paper is organized as follows. Section 2 briefly describes all key methods used in the present study. Section 3 discusses the major features how to infer absolute concentrations from measured slant column amounts from O_3, NO_2, and BrO, namely the optimal estimation technique, and of our novel O_3-scaling technique together with their sensitivity to various input and model parameters. In section 4, the major observations are presented and discussed along with the amount of inorganic bromine present within the TTL. Further implications of our measurements for the photochemistry of bromine and ozone within the TTL and lowermost subtropical stratosphere are discussed. Section 5 concludes the study.

2 Methods

The instruments of the NASA-ATTREX package most important for the present study consists of a fast UV photometer for measurement of ozone (Gao et al., 2012), a gas chromatograph (UCATS, Wofsy et al. (2011) and Moore et al. (2003)) as well as a Picarro instrument (HUPCRS, Crosson (2008), Rella et al. (2013), and Chen et al. (2013)) to measure CH_4, CO_2, and CO, a whole air sampler (GWAS, Schauffler et al. (1998) and Schauffler et al. (1999)) to analyze a large suite of stable trace gases, and a 3-channel scanning limb mini-DOAS instrument for spectroscopic detection of O_3, NO_2, BrO, OClO, IO, O_4, O_2,

H_2O_{vapor}, H_2O_{liquid}, and H_2O_{solid} in the UV/vis/near-IR spectral ranges (e.g., Weidner et al. (2005), Platt and Stutz (2008), Kritten et al. (2010), Kreycy et al. (2013), Kritten et al. (2014), Stutz et al. (2016), and others).

In following all instruments, techniques, methods, and tools are briefly described.

2.1 DOAS measurements of O_3, NO_2, and BrO

The mini-DOAS instrument is a UV/vis/near-IR 3-channel optical spectrometer by which scattered skylight received from limb direction and direct sunlight can be analyzed for a large number of atmospheric species, including O_3, NO_2, and BrO. Since the instrument and retrieval methods are described in detail in the accompanying paper by Stutz et al. (2016) (for further details see Table 2 therein), only some key elements of the data analysis are described here.

The post-flight analysis of the collected data for the detection of O_3, O_4, NO_2, and BrO and concentration retrieval include (a) the spectral retrieval of the targeted gases using the DOAS method (Platt and Stutz, 2008) (for the DOAS settings see Table 4 in Stutz et al. (2016)), (b) forward RT-modeling of each observation using the Monte Carlo model McArtim (Deutschmann et al., 2011) (for further details see section 2.6), and (c) for the concentration and profile retrieval either the non-linear optimal estimation (Rodgers, 2000), or the novel x-gas scaling technique (for details see sections 4.2. and 4.3 in Stutz et al. (2016)). Typical errors are ± 5 ppb for O_3, ± 15 ppt for NO_2, and ± 0.5 ppt for BrO, to which possible systematic errors in the individual absorption cross section need to be added. These are for O_3-UV $\pm 1.3\%$, O_3-vis $\pm 2\%$, NO_2 $\pm 2\%$, and BrO $\pm 10\%$, respectively (for more details of error budget see Stutz et al. (2016)).

2.2 In-situ measurements of O_3

The NOAA-2 polarized O_3 photometer (Gao et al., 2012) is a derivative of the dual-beam, unpolarized, UV absorption technique described by Proffitt and McLaughlin (1983). Briefly, the ambient and O_3-free air flow is alternately directed into two identical 60 cm long absorption cells. The 253.7-nm UV light from a mercury lamp is split into two beams that are each directed into one of the absorption cells. Since O_3 strongly absorbs 253.7-nm photons, the UV beam passing through the cell containing ambient ozone is attenuated more than the beam passing through the cell containing O_3-free air. Knowing the O_3 absorption cross section ($\sigma(O_3)$) and the absorption path length (L), the O_3 partial pressure ($p(O_3)$) in the ambient air can be derived using Beer's law.

The instrument has a fast sampling rate (2 Hz at $<$ 200 hPa, 1 Hz at 200 to 500 hPa, and 0.5 Hz at $\geq$ 500 hPa), high accuracy (3% excluding operation in the 300 - 450 hPa range, where the accuracy may be degraded to about 5%), and excellent precision (1.1×10^{10} O_3 molecules/cm^3 at 2 Hz, which corresponds to 3.0 ppb at 200 K and 100 hPa, or 0.41 ppb at 273 K and 1013 hPa). The size (36 l), weight (18 kg), and power (50 - 200 W) make the instrument suitable for many unmanned aerial vehicle systems (UAS) and other airborne platforms. In-flight and laboratory inter-comparisons with existing O_3 instruments have shown that measurement accuracy (3 %) is maintained in flight.

2.3 CH_4 measurements by UCATS

The Unmanned aircraft system Chromatograph for Atmospheric Trace Species (UCATS) measures atmospheric methane (CH_4) on one gas chromatographic channel along with hydrogen (H_2) and carbon monoxide (CO) once every 140 seconds. UCATS has two chromatographic channels with electron capture detectors (ECDs), two ozone (O_3) ultraviolet absorption spectrometers, and a water vapor (H_2O) tunable diode laser absorption spectrometer (TDLAS). The details of the CH_4 chromatography are similar to those on our balloon and airborne instruments described in (Moore et al. (2003) and Elkins et al. (1996)). The addition of 100 ppm of nitrous oxide to the make-up line of the ECD enhances the sensitivity to H_2, CO, and CH_4 (Elkins et al. (1996) and Moore et al. (2003)). The separation of these gases in air is accomplished with pre-column of Unibeads (2 m × 2 mm diameter), and a main column of Molecular Sieve 5A (0.7 m × 2.2 mm diameter) at $\sim$ 110 °C (Moore et al., 2003). The precision of the CH_4 measurement during ATTREX was ±0.5% and is calibrated during flight with a secondary standard after every three ambient air measurements. Instrumental drift is corrected between the standard injections. UCATS measurements are traceable to the WMO Central Calibration Laboratory (CCL) and are on the CH_4 WMO X2004A scale (Dlugokencky et al. (2005), with update given at http://www.esrl.noaa.gov/gmd/ccl/ch4_scale.html).

2.4 CH_4 measurements by HUPCRS

The Harvard University Picarro Cavity Ringdown Spectrometer (HUPCRS) consists of a G2401-m Picarro gas analyzer (Picarro Inc., Santa Clara, CA, USA) repackaged in a temperature-controlled pressure vessel, a separate calibration system with 2 multi-species gas standards, and an external pump and pressure control assembly designed to allow operation at a wide range of altitudes. The Picarro analyzer uses Wavelength-Scanned Cavity Ringdown Spectroscopy (WS-CRDS) technology to make high precision measurements of greenhouse gases (Crosson (2008), Rella et al. (2013), and Chen et al. (2013)). HUPCRS reports concentrations of CO_2, CH_4, and CO every $\sim$ 2.2 seconds and the data are averaged to 10 seconds. In-flight precision for CH_4 is 0.2 ppb in 10 seconds.

Briefly, the analyzer uses three distributed feedback (DFB) diode lasers in the spectral region of 1.55 to 1.65 μm. Monochromatic light is injected into a high-finesse optical cavity with a volume of 35 cm^3 and a configuration of three highly reflective mirrors ($\leq$ 99.995%). Internal control loops keep the cavity at 140 ± 0.02 Torr and 45 ± 0.0005 °C in order to stabilize the spectra. The injected light is blocked periodically and when blocked, the exponential decay rate of the light intensity is measured by a photo-detector. The decay rate depends on loss mechanisms within the cavity such as mirror losses, light scattering, refraction, and absorption by a specific analyte. A sequence of specific wavelengths for each molecule is injected into the cavity in order to reconstruct the absorption spectra. A fit to the spectra is performed in real time and concentrations are derived based on peak height. High-altitude sampling (i.e. very low pressure and temperature) necessitated transferring the core components of the Picarro analyzer to a sealed tubular pressure vessel, which is maintained at 35 ° C and 760 Torr. The analyzer's components are isolated from the pressure vessel to provide vibration damping and decoupling from deformations in the pressure vessel caused by external pressure changes.

The sampling strategy for HUPCRS consists of bringing in air through a rear-facing inlet, filtered by a 2 μm Zefluor membrane, and dehydrating this air by flowing it through a multi-tube Nafion followed by a dry-ice cooled trap prior to entering the Picarro analyzer. A choked upstream Teflon-lined diaphragm pump delivers ambient air to the analyzer at 400 Torr, regardless of aircraft altitude, via a flow bypass. A similar downstream pump, with an inlet pressure of 10 Torr, facilitates flow through the analyzer at high altitude and ensures adequate purging of the Nafion drier. Measurement accuracy and stability are monitored by replacing ambient air with air from two NOAA-traceable gas standards (low- and high-span) for a total of four minutes every 30 minutes. These standards are contained in 8.4 liter carbon fiber wrapped aluminum cylinders and housed in a temperature-controlled enclosure. The total weight of the package is 97 kg.

2.5 The GH Whole Air Sampler (GWAS)

The Global Hawk Whole Air Sampler (GWAS) is a modified version of the Whole Air Sampler used on previous airborne campaigns (Heidt et al. (1989), Schauffler et al. (1998), Schauffler et al. (1999), and Daniel et al. (1996)). Briefly, the instrument consists of 90 custom-made canisters, Silonite-coated (Entech Instruments, Simi Valley, CA) of 1.3 liter, controlled with Parker Series 99 solenoid valves (Parker-Hannifin, Corp., Hollis, NH). Two metal bellows compressor pumps (Senior Aerospace, Sharon, MA) allow the flow of ambient air through a custom inlet at flow rates ranging from 2 to 8 standard liters/minute, depending on altitude. The manifold and canister module temperatures are controlled to remain within the range of 0 - 30 °C. GWAS is a fully automated instrument controlled from the ground through an Ethernet interface. Parameters to fill the canisters, flush the manifold, and control the temperature, are pre-determined in the Data System Module (DSM) inside the aircraft, to fill the canisters automatically in case of failure of the aircraft networks. However, during the entire flight, the parameters are manually set with the ground laptop computer to improve the sampling collection at different altitudes. During the ATTREX campaign, the canisters were filled to $\sim$ 3 standard atmosphere (40 psi) in about 25 sec at 14 km and 90 sec at 18 km. The samples are analyzed using a high performance gas chromatograph (Agilent Technology 7890A) and mass spectrometer with mass selective, flame ionization and electron capture detector (Agilent Technology 5975C). Samples are concentrated on an adsorbent tube at -38 °C with a combination of cryogen-free automation and thermal desorber system (CIA Advantage plus UNITY 2, Markes International). The oven temperature profile is -20 °C for 3 min, then 10 °C/min to 200 °C and 200 °C for 4 min, for a total analysis time of 29 min. Under these sampling conditions the precision is compound/concentration dependent, and ranged from $\leq$2% to 20%. Calibration procedures as well as mixing ratios calculations are described elsewhere (Schauffler et al., 1999).

2.6 Radiative transfer modeling

The received limb radiances are modeled in spherical 1D, and in selected cases in 3D, using version 3.5 of the Monte Carlo radiative transfer (RT) model McArtim (Deutschmann et al., 2011). The model's input is chosen according to the on-board measured atmospheric temperatures and pressures, including climatological low latitude aerosol profiles from SAGE III (http://www.eosweb.larc.nasa.gov/PRODOCS/sage3/table-/sage3.htm), and lower atmospheric cloud covers as indicated by the cloud physics lidar measurements made from aboard the GH (see http://cpl.gsfc.nasa.gov/). In the standard run, the ground (oceanic) albedo is set to 0.07 in UV, and 0.2 in visible spectral range. The RT model is further fed with the actual geolocation of the GH, solar zenith and azimuth angles as encountered during each measurement, the telescopes azimuth and elevation angles, as well as the field of view (FOV) of the mini-DOAS telescopes. Fig. 5 in Stutz et al. (2016) displays one example of an RT simulation for limb measurements at 18 km altitude. The simulation demonstrates that the Earth's sphericity, the correct treatment of atmospheric refraction, cloud cover, ground albedo etc. are relevant in the context of the UV/vis/near-IR limb measurements within the middle atmosphere (Deutschmann et al., 2011). Even though the 3 (UV/vis/near-IR) mini-DOAS spectrometers are not radiometrically calibrated on a absolute scale, past comparison exercises of measured and McArtim modeled limb radiance provide confidence on the quality of the RT simulations (e.g., see Fig. 5 and Fig. 6 in Deutschmann et al. (2011) and Fig. 2 in Kreycy et al. (2013)).

For the simulations of the trace gas absorptions measured in limb direction, the RT model is further fed with TOMCAT/SLIMCAT simulated curtains of the targeted gases simulated along the GH flight paths (see section 2.7).

2.7 Photochemical modeling

For the interpretation of our measurements, we use simulations of the TOMCAT/SLIMCAT 3-D chemical transport model (CTM) (Chipperfield (1999), and Chipperfield (2006)). More specifically, the simulations are used for inter-comparison with measured photochemical species, for assessment of the budget of $\mathrm{Br_y^{inorg}}$, and for sensitivity studies on the impact of our measurements on the photochemistry of bromine and ozone in the subtropical UT/LS, tropical UT, and TTL.

For the present study the TOMCAT/SLIMCAT model is driven by meteorology from the ECMWF ERA-interim reanalyses (Dee et al., 2011). The reanalyses are used for the large-scale winds and temperatures as well as convective mass fluxes (Feng et al., 2011). The model has a detailed stratospheric chemistry scheme with kinetic and photochemical data taken from JPL-2011 Sander et al. (2011) with recent updates. The model chemical fields are constrained by specified time-dependent surface mixing ratios. For the brominated species, the following surface mixing ratios of stratospheric-relevant source gases are assumed: $[\mathrm{CH_3Br}] = 6.9$ ppt, [halons]= 7.99 ppt, $[\mathrm{CHBr_3}] = 1$ ppt, $[\mathrm{CH_2Br_2}] = 1$ ppt, and $\Sigma\,[\mathrm{CHClBr_2, CHCl_2Br, CH_2ClBr, ...}]$ = 1 ppt of Br, which together contain 1 ppt of bromine atoms. Organic bromine is thus $[\mathrm{Br_y^{org}}]$ = 20.89 ppt at the surface, in agreement with recent reports (e.g., WMO (2014), Sala et al. (2014)). No other (c.f., unknown organic or inorganic) sources of bromine for UT, LS, and TTL are assumed (e.g., Fitzenberger et al. (2000), Salawitch et al. (2010), Wang et al. (2015), and others), except that we add 0.5 ppt to the modeled tropospheric BrO in agreement with the finding discussed below (section 4.6). The surface concentration of $\mathrm{CH_4}$ is specified based on observations of AGAGE (https://agage.mit.edu/) and NOAA, which reflect recent variations in its growth rate.

The standard model run (#583) is initialized in 1979 and spun-up for 34 years at low horizontal resolution (5.6° × 5.6°) and with 36 unevenly spaced sigma-pressure vertical levels in the altitude range 0 - 63 km. Output from January 1, 2013 is interpolated to a high horizontal resolution (1.2° × 1.2°) and the simulation continued over the ATTREX campaign period using this resolution. The model output is sampled on-line along the Global Hawk flight tracks for direct comparison with the observations. Two further high resolution sensitivity experiments are performed from January 1, 2013 onwards. In run #584, the ratio of the photolysis frequency of $\mathrm{BrONO_2}$ and the three-body association rate reaction coefficient $k_{\mathrm{BrO+NO_2}}$ is increased by a factor 1.75 (e.g., Kreycy et al. (2013)). In run #585 the second-order rate reaction coefficient k_{Br+O_3} is set to the upper limit of its uncertainty range (Sander et al. (2011)).

For all model levels and for the time resolution (∼30 s) of the mini-DOAS measurements, 'curtains' of the targeted gases along the flight track are stored (e.g., see Fig. 6 in Stutz et al. (2016) and Fig. 2 in this study). They are imported into the radiative transfer model McArtim for further forward simulations of the observations, and measurement versus model intercomparison studies. The inclusion of simulated TOMCAT/SLIMCAT curtains in our study is particularly necessary for (a) the retrieval of absolute concentrations using the O_3-scaling technique (see Stutz et al. (2016), section 4.3), (b) estimate of errors and retrieval sensitivities to various parameters (see section 4.4 and the supplement to Stutz et al. (2016)), (c) the separation of dynamical and photochemical processes in the interpretation of our data, (d) sensitivity tests for the assumed kinetic data, and (e) the assessment of total Br_y^{inorg} (see section 4).

3 Measurements and data reduction

Within the framework of the NASA-ATTREX project, the Global Hawk performed 6 flights into the subtropical LS, UT, and TTL over the Eastern Pacific in early 2013 (Fig. 1) and another 9 flights over the Western Pacific in early 2014. The present paper reports on the 2013 flights, since the 2014 flights were mostly performed into the cold TTL, where cirrus clouds mostly prevailed at flight level. Evidently due to the multiple scattering of light by the cirrus cloud particles, the interpretation of our UV/vis limb measurements is not straightforward. Accordingly the data collected in 2014 will be reported elsewhere in a future work. Details of the NASA-ATTREX 2013 instrument package, the flights, some exciting observations and details on the collected data can be found in the articles of Jensen et al. (2013) and Jensen et al. (2015), on the project's website https://espo.nasa.gov/missions/attrex/content/ATTREX .

In February and March 2013, the NASA-ATTREX flights of the Global Hawk were strongly biased with respect to the sampled air masses, mostly because the scientific interest was primarily put on probing the TTL over the Eastern Pacific for aerosols and cirrus cloud particles during the convective season, rather than for the photochemistry of bromine in the LS, UT, and TTL (see Fig. 1). Therefore, and due to operational reasons typical flight patterns extended from Dryden/California into southern or south-western direction during daytime until a turn-point was reached and the back leg to Dryden in north-eastern direction occurred during the night, when the mini-DOAS instrument could not take measurements. The dives were mostly performed within the TTL, and occasionally within the subtropical lowermost stratosphere during the return legs at night but not during the out-going daytime legs. Finally the landings at Dryden were scheduled for the early local morning, mostly due to operational constraints. Therefore, no profiles of the targeted species could be obtained in the subtropical lowermost stratosphere at daytime, but a large number within the UT and TTL.

Furthermore, the latitudinal definition of the notations 'subtropical' LS and 'tropical' TTL need some clarification. According to the definition of Fueglistaler et al. (2009), the latitudinal boundary between the subtropics and tropics should be where the subtropical jet is located. However, since we do not infer dynamical parameters (such as the potential vorticity) from our data, we conveniently define the boundary according to proxies for (a) different air mass ages, i.e. $[CH_4]$ concentrations

$\leq$ 1390 ppb are labeled 'subtropical' and [CH_4] $\geq$ 1390 ppb) are labeled 'tropical', and (b) photochemical regimes, i.e. [O_3] (subtropical when [O_3] $\geq$ 150 ppb, and TTL when [O_3] $\leq$ 150 ppb), which we find suitable from a visual inspection of our data (see below).

As mentioned above and outlined in detail in the study of Stutz et al. (2016), the processing of the mini-DOAS data included (a) spectral retrieval of the targeted gases from the mini-DOAS measurements (section 2.1), (b) forward modeling of the radiative transfer for each measured spectrum (section 2.6), and either applying optical estimation or the novel x-gas scaling technique (see sections 4.1 and 4.2 in Stutz et al. (2016)). Comprehensive sensitivity simulations indicated that optical estimation based on constraints inferred from measured O_4 and/or relative radiance would not result in the desired error range (Stutz et al. (2016), section 4.2). Therefore we decided to apply the x-gas scaling technique (Stutz et al. (2016) and Raecke (2013)) with x being ozone measured in-situ by the NOAA-2 O_3 photometer (see section 2.2).

The O_3-scaling technique makes use of the in-situ O_3 measured by the NOAA instrument (Gao et al., 2012) and the limb measured O_3 total slant column amounts (SCD_{O3}) either monitored in the UV (for the retrieval of BrO in the 343 - 355 nm wavelength band) or visible wavelength range (for the retrieval of NO_2 in the 424 - 460 nm wavelength band) (see equation 12 in Stutz et al. (2016)). Here the ratio of the measured slant column and in-situ measured SCD_{O3}/[O_3] can be regarded as a proxy for the (horizontal) light path length over which the absorption is collected. In fact in the paper of Stutz et al. (2016), it is argued that the so-called α factors account for the fraction of the absorption of the scaling gas x (e.g., x = O_3 in our study) picked-up on the horizontal light paths ahead of the aircraft relative to the total measured absorption. The sensitivity study on the α factors presented in Stutz et al. (2016) (e.g., in the supplement) indicates that for the targeted gases uncertainties in α factor ratios due to assumptions regarding the radiative transfer (for example due to Mie scattering by aerosols and clouds) mostly cancel out, while uncertainties in the individual profile shapes of the targeted and scaling gas are most relevant for the errors of the inferred gas concentrations. Therefore in the present study, profile shapes of the targeted and scaling gas predicted by the TOMCAT/SLIMCAT CTM are used in the radiative transfer calculations, aiming at the calculation of the α factors. The uncertainties in the profile shapes (assumed to be of the order of the altitude adjustment of the CH_4 and O_3 curtains, which are typically much smaller than the altitude grid spacing in the SLIMCAT/TOMCAT simulations) are then carried over to calculate the overall errors, as discussed in section 4.4 of the Stutz et al. (2016) study.

It should be noted that, for the flight on Feb. 21, 2013 (SF4-2013), the DOAS retrieval is much less robust than for all the other flights, most likely because the Fraunhofer reference spectra (taken via a diffuser) are affected by temporally changing residual structures likely due to ice deposits or some other residues on the entrance diffuser. Therefore the data of this flight are not analyzed in detail, but they are only reported for completeness here.

Finally, in our analysis only those data which are taken at a solar zenith angle (SZA) $\leq 88\,^\circ$ are considered, because for increasing SZAs the received skylight radiance requires increasingly longer signal integration times, and are thus averaged over longer distances ahead of the aircraft. Moreover, as the SZA increases the skylight is expected to traverse an increasingly inhomogeneous curtain of the probed radicals (e.g., inspect Figs. 5, and 6 in Stutz et al. (2016)). As consequence, the spatial grid of TOMCAT/SLIMCAT ($1.2 \times 1.2\,^\circ$) on which the photochemistry is simulated appeared too coarse for a useful interpretation of our measurements at large SZAs. Therefore for a tighter interpretation of our data, a model with higher spatial resolution than provided by TOMCAT/SLIMCAT would be required. Such an approach is for example followed in the balloon-borne studies of Harder et al. (2000), Butz et al. (2009), and Kreycy et al. (2013), and others. However, since both processes are likely to increase the error of our analysis, and since large SZA ($\geq 88^o$) measurements only constitute a minor part of all measurements, we refrain from this much more complicated approach.

4 Results and Discussion

In this section we first discuss how our mini-DOAS measurements of O_3, NO_2, and BrO, as well as of CH_4 (from UCTAS and HUPCRS), and of the organic brominated source gases (from GWAS) compare with the model predictions of the TOMCAT/SLIMCAT model (sections 4.1 and 4.2). Then measured BrO is compared with previous measurements in the UT/TTL/LS (section 4.3), and with the model predictions (section 4.4). Uncertainties and errors in the inferred Br_y^{inorg} are assessed (section 4.5), before implications of our measurements for total Br_y (section 4.6), and impacts of our measurements for TTL ozone are discussed (section 4.7).

4.1 Comparison with TOMCAT/SLIMCAT predictions

Figures 4 to 9 provide overviews on the measured data together with the TOMCAT/SLIMCAT modeled Br_y^{inorg} partitioning (panels f) and inferred total Br_y^{inorg} (panels g) as a function of universal time for each flight. The modeled values are obtained by linear interpolation of the curtain data (see Fig. 2) to the exact altitude of the GH.

The panels (b), and (c) of Figs. 4 to 9 show comparisons of measured and modeled CH_4, and O_3 mixing ratios. Here the measured and modeled species agree excellently within the given error bars, after the modeled curtains are altitude-adjusted (for details see Stutz et al. (2016)). The excellent agreement achieved between measured and modeled CH_4, and O_3 lends confidence that the altitude-adjusted TOMCAT/SLIMCAT model fields reproduce well the essential dynamical and photochemical processes of the probed air masses. The quality of the dynamical simulations are further tested by comparing modeled and measured O_3 as a function of CH_4 (Fig. 10). For all flights the agreement of the observed and modeled O_3 vs CH_4 correlation is reasonably good, except for flights SF1-2013 and SF2-2013, where the UCATS measured CH_4 scatters around the simulated CH_4 concentrations. This scatter is most likely due to calibration errors of UCATS, rather than reflecting the real behavior of the atmosphere. Evidence for this conclusion is provided from the CH_4 comparisons for SF3-2013 to SF6-2013, in which the HUPCRS CH_4 data are taken; these data do not show such a scatter and compare well with the model predictions.

Panels (d) of Figs. 4 to 9 compare measured and modeled NO_2. Overall the measured (and modeled) NO_2 concentrations meet the expectations for NO_x (= NO + NO_2 + NO_3) abundances in the LS, UT, and TTL over the pristine Pacific. Elevated NO_2 concentrations (range 70 to 170 ppt) are measured within the subtropical lowermost stratosphere, where aged air masses are probed, as indicated by depleted CH_4 concentrations and elevated O_3 concentrations (and presumably decreased N_2O concentrations). Note that N_2O is the primary source for stratospheric NO_x, and in the stratosphere CH_4 and N_2O destruction closely follow each other (e.g., Michelsen et al. (1998), Ravishankara et al. (2009)). Very low NO_2 concentrations ($\leq$ 30 ppt) are detected within the UT and TTL, indicating that the analyzed air does not originate from recently polluted, or lightningaffected regions. Further, the modeled NO_2 concentrations (red line in panel d) are found to fall into the given range of errors of the measured NO_2 concentrations. This finding strongly indicates that, the NO_x and NO_y (= NO_x, N_2O_5, $HONO_3$, HO_2NO_2,...) budget and photochemistry of the LS, UT, and TTL are reproduced well in the TOMCAT/SLIMCAT simulations, and that overall the O_3-scaling technique works well for NO_2.

4.2 Comparison of measured and model organic bromine

Before measured and modeled BrO can be compared quantitatively, it is necessary to compare the measured amounts of different brominated source gases with the model predictions (Fig. 11). For the assumed (constant) surface concentrations (see subsection 2.7), measured and modeled CH_3Br (upper left panel), $CHBr_3$ (upper right panel), and for all other halons, for example H1211 (lower right panel), compare well, even if the data is scattered from flight to flight. For CH_2Br_2, however, TOMCAT/SLIMCAT run # 583 underpredicts the observed mixing ratio for high concentrations (by 0.1 ppt) and overpredicts it by up to 0.2 ppt for low concentrations (lower left panel). This is most likely due to an assumed too low surface concentration (1.05 ppt), and errors the atmospheric lifetime by reactions of CH_2Br_2 with OH radicals in the model (e.g. Mellouki et al. (1992), Ko et al. (2013), WMO (2014)).

The flight-to-flight and sample-to-sample scatter in CH_3Br, and $CHBr_3$ is mostly due to different source regions of the air masses probed during SF1-2013 to SF6-2013. This implies a spatially (and possibly time-dependent) varying source strength of the brominated natural source gases to be implemented in the model (e.g., Hossaini et al. (2013), Ziska et al. (2013), and others). In the present version of the TOMCAT/SLIMCAT simulations, this scatter introduces an estimated uncertainty of ± 0.8 ppt into Br_y^{org}, and potentially in the inferred Br_y^{inorg} available in the TTL. The systematic under-prediction of 0.1 ppt at high CH_2Br_2 concentrations, and its too long lifetime in the TTL leading to too large CH_2Br_2 concentrations in the model for old air (by up to 0.2 ppt) may cause an additional and systematic under-prediction of Br_y^{inorg} of up to ≤ 0.4 ppt in the model. Both contributions to the uncertainty in the Br_y^{org} are considered when comparing measured and modeled BrO, and Br_y^{inorg} (see below).

4.3 Comparisons of measured BrO with previous studies

Next, we compare our data with previous BrO measurements in the UT and TTL, i.e. the balloon measurements of Dorf et al. (2008), and the aircraft measurements of Wang et al. (2015) and Volkamer et al. (2015) during the TORERO campaign.

Overall the balloon-borne BrO profile measurements of Dorf et al. (2008) performed over tropical Brazil during the dry (i.e. the non-convective season) in June 2005 and June 2008 compare excellently with the BrO profiles inferred from our measurements for the UT and TTL (i.e. typically [BrO] = 0.5 -1.0 ppt in the upper UT and base of the TTL, and up to 5 ppt at the cold point tropopause (e.g., compare Fig. 1 in Dorf et al. (2008) with Fig. 3).

The present study and the BrO profile measurement of Dorf et al. (2008) are, however, in contrast to recent reports on the presence of BrO amounting up to 3 ppt in the tropical and subtropical UT, and around the bottom of the TTL (Wang et al., 2015) (compare Fig. 2, panel A in Wang et al. (2015) with panel (c) in Fig. 3). Here we emphasize again that we find no indications for unexpected high or elevated BrO concentrations in the UT, and TTL, either from inspecting the UT from above (e.g., see Fig. 15 in Stutz et al. (2016)), nor when directly probing the TTL (see Figs. 3 to 9).

Several similarities and differences exist between the Wang et al. (2015) and our study. Using NSF/NCAR G-V, Wang et al. (2015) probed the UT and the bottom of the TTL (up to about 14 km) for BrO over an adjacent part of the Pacific, i.e. mostly off the western coasts of South and Central America, but more to the south than probed during the present study, but notably during the same season. So it could be just a matter of chance, or due to the different regions probed in both studies that we missed detecting elevated BrO concentration in the UT and the bottom of the TTL.

Second, even though Wang et al. (2015) use a technique similar to us in the present study, and in particular they use the same radiative transfer code (e.g., McArtim see Deutschmann et al. (2011)) for the interpretation of their measurements, they were using the optimal estimation technique to retrieve the BrO profiles (Volkamer et al., 2015). It is known that the optimal estimation technique may deliver robust results if the region of interest is carefully sampled, and if the so-called forward model describes reasonably well the physical reality (Rodgers, 2000). Accordingly, Wang et al. (2015), and Volkamer et al. (2015) invested significant effort to constrain well their radiative transfer, for example by using information on the aerosol type and their optical properties gained by other instrumentation and/or by constraining the radiative transfer with measured information on the absorption of the O_2-O_2 collisional complex (see Fig. 3 in Volkamer et al. (2015)). Our study on the sensitivity of the O_2-O_2 absorption measured in limb direction as function of the cloud cover underneath (see sections 4.2 and Fig. 7 in Stutz et al. (2016)) as well as the results presented by Volkamer et al. (2015) (in their Fig. 3) clearly demonstrates the limitation of the O_2-O_2 method to constrain the radiative transfer for UV/vis studies above an altitude 10 km, mostly because the bulk of the O_2-O_2 collisional complex is located near the surface. Therefore, any skylight analyzed for the O_2-O_2 absorption in limb direction may carry additional, or even predominantly information on the radiative transfer of lower atmospheric layers (see Figure 7 in Stutz et al. (2016)), rather than of the targeted atmospheric layers.

Furthermore, Wang et al. (2015), and Volkamer et al. (2015) did not use a stratospheric CTM to study the potential influence of changing overhead BrO concentrations on their results. As result, the predominant occurrence of atmospheric BrO in the stratosphere at daytime, and its potential column changes mostly due to a changing tropopause height (e.g., at the subtropical or polar jet) may mimic the presence of BrO in limb the direction, or at flight altitude (e.g., Wang et al. (2015), and Volkamer et al. (2015) and Fig. 14 in Stutz et al. (2016)).

In conclusion, even though the reported TORERO flights 12 and 17 were performed under clear-skies (Volkamer et al., 2015), it is unclear the extent to which unaccounted scattering due to aerosols and (probably) optically thin upper tropospheric clouds, lower level clouds, or changing overhead stratospheric BrO contributed to the inferred (or by error attributed) elevated BrO in the UT, and around the bottom of the TTL.

4.4 Comparison of measured and modeled BrO

Measured and modeled BrO are displayed in Figs. 4 to 9 (panel e), together with the modeled $\mathrm{Br_y^{inorg}}$ partitioning (panel f) and inferred $\mathrm{Br_y^{inorg}}$ (panel g). Again elevated BrO concentrations are measured within the LS (range 3 - 9 ppt), and lower BrO concentrations in the TTL (range 0.5 - 5 ppt), with the smallest BrO concentrations (0.5 - 1 ppt) occurring near the bottom of the TTL. Overall this behavior is expected from arguments based on the amount and composition of the brominated organic and inorganic source gases, their lifetimes, and atmospheric transport (e.g., Fueglistaler et al. (2009), Aschmann et al. (2009), Hossaini et al. (2012b), Ashfold et al. (2012), WMO (2014), and others).

With these features in mind, Fig. 12 compares measured and modeled BrO. For the majority of all flights (except flight SF4-2014, for which a DOAS retrieval problem exists which causes a bias of 2 ppt in inferred BrO), measured and modeled BrO compare excellently for low concentrations (i.e. close to bottom to the TTL), or very young air. For larger BrO concentrations (and older air) good agreement between the measurement and model is found for SF1-2013, SF5-2013, and SF6-2013, when mostly air of low NO_2 concentrations (and predicted low $BrONO_2$ concentrations) is probed. For large BrO concentrations as encountered during flights SF2-2013, and SF3-2013, the measured BrO is up to 2 ppt, or 25% larger than what the model predicts. This gap could partly be closed by adjusting the CH_2Br_2 surface concentration and atmospheric lifetime. Adjusting CH_2Br_2 thus would add 0.4 ppt of Br_y^{inorg}, or $\sim$ 0.3 ppt to BrO, thus removing the flight-to-flight scatter in source gas concentrations (± 0.8 ppt) in Br_y^{inorg}. This could for example be done by a detailed back trajectory and source appointment analysis to which a forthcoming study well be devoted.

4.5 Uncertainties in estimating the inorganic bromine partitioning

Another reason for the gap in measured and modeled BrO may come from uncertainties in the used kinetic constants and how they affect the Br_y^{inorg} (= Br + BrO + $BrONO_2$ + HOBr + HBr) partitioning. Our photochemical modeling, aimed at reproducing measured O_3, NO_2, and BrO (see the panels (f) in Fig. 4 to Fig. 9), indicates that at daytime HOBr and HBr contribute less than 10% to Br_y^{inorg}. Therefore, we concentrate on the photochemical model errors due to the partitioning primarily among BrO, Br, and $BrONO_2$. In this context, most important are the reactions $BrO + NO_2 + M \rightarrow BrONO_2 + M$ followed by the photolysis of $BrONO_2$, and the reaction $Br + O_3 \rightarrow BrO + O_2$.

How uncertainties of the photolytic destruction (J) and three-body formation reaction (k) (together referred to as J/k) of $BrONO_2$ propagate into BrO is tested in model run #584. Here, according to the finding of Kreycy et al. (2013) J/k was increased by a factor 1.7 (+0.4/-0.2) as compared to the JPL recommendation (Sander et al., 2011) (see the blue crosses in Fig. 12). Evidently increasing J/k helps to close the remaining gap in measured versus modeled BrO, which becomes particularly relevant to reproduce BrO when NO_2 is large, i.e. in the subtropical LS.

Furthermore, Sander et al. (2011) estimate the uncertainty in the reaction rate coefficient k_{Br+O3} at low temperature (T = 190 K) to be ± 40% (see comment G31). When only considering the two studies which actually measured rather than extrapolated the reaction rate coefficient into the relevant temperature range (T = 190 - 200 K), smaller uncertainty (28%) is indicated (Michael et al. (1978) and Nicovich et al. (1990)). Therefore, in the following an uncertainty of 28% for Δk_{Br+O3} is assumed. Overall, increasing k_{Br+O3} (model run #585) to the upper limit possible according to the JPL compilation (i.e. by factor of 1.28) changes the measured vs modeled correlation for BrO very little (see the red crosses in Fig. 12). It does change, however, the Br_y^{inorg} partitioning so that [BrO] is always largely prevalent over [Br] even at the lowest altitudes of the TTL (e.g., see panel (f) in Fig. 4 to 9). Our joint measurement of O_3, NO_2, and BrO and the supporting CTM simulations thus indicate $[Br]/[BrO] < 1$ for all probed regimes. Our finding is therefore in contrast to the simulations of Fernandez et al.

(2014), and Saiz-Lopez and Fernandez (2016) who suggest that $[\mathrm{Br}]/[\mathrm{BrO}]$ may become larger than unity in the tropical UT and TTL at daytime. This conclusion is due mostly to the larger measured $\mathrm{O_3}$ concentrations than those modeled in the study of Fernandez et al. (2014) and Saiz-Lopez and Fernandez (2016), and the conclusion is irrespective of what (within the given error bars) is assumed for $\mathrm{k_{Br+O3}}$.

Gaussian addition of all uncertainties and errors (i.e. the errors of the retrieved BrO concentrations (in section 4.4 of Stutz et al. (2016)), the cross section error, and the uncertainty in the modeled $[\mathrm{Br}]/[\mathrm{BrO}]$, and $[\mathrm{BrONO_2}]$/[BrO] ratios), leads to the $\mathrm{Br_y^{inorg}}$ error, as indicated in the panel (f) of Figs. 4 to 9.

4.6 Inferred total $\mathrm{Br_y^{inorg}}$

Finally, we discuss the inferred $\mathrm{Br_y^{inorg}}$ (contribution 4) as function of potential temperature in the LS, UT, and TTL over the Eastern Pacific during the 2013 convective season (Figure 13). Here we discriminate between young air $[\mathrm{CH_4}] \geq 1790$ ppb, mostly found within the tropical UT and TTL (Fig. 13, left panel), and older air $[\mathrm{CH_4}] \leq 1790$ ppb (Fig. 13, right panel) mostly found in the subtropical lowermost stratosphere. The different histograms in Fig. 13 clearly indicate that, $\mathrm{Br_y^{inorg}}$ increases with increasing potential temperature i.e. from 2.63 ± 1.04 ppt at θ = 350 - 360 K (at the bottom of the TTL) to 4.22 ± 1.37 ppt for θ = 390 - 400 K (just above the cold point tropopause). The inferred $\mathrm{Br_y^{inorg}}$ thus brackets well the model $[\mathrm{Br_y^{inorg}}]$ = 3.02 ± 1.90 ppt predicted to exist at 17 km in the TTL (Navarro et al., 2015).

The increase in $\mathrm{Br_y^{inorg}}$ with increasing potential temperature θ and decreasing $\mathrm{CH_4}$ concentration thus reflects the decrease in concentrations of brominated VSLS (contribution 3). The correspondence of decreasing $\mathrm{Br_y^{org}}$, and increasing $\mathrm{Br_y^{inorg}}$ concentrations is also found on a sample-to-sample as well as on flight-to-flight basis. This correspondence keeps $[\mathrm{Br_y}]$ almost constant within the TTL during an individual flight, but $[\mathrm{Br_y}]$ varies from flight-to flight in a range of $[\mathrm{Br_y}]$ = 20.3 ppt to 22.3 ppt (Figure 14).

Moreover, it appears that the increase in $\mathrm{Br_y^{inorg}}$ with θ mostly corresponds to a decrease in concentrations of the brominated VSLS, however, only if the same (young) air masses of large $\mathrm{CH_4}$ concentrations are probed (Figure 15). For example for SF1-2013, SF5-2013, and SF6-2013 when mostly TTL is probed, all data points fall into a band of about ±1 ppt in width, next to a flight-dependent diagonal line (not shown), but not for SF3-2013 when the LS (and thus older air) and TTL is probed. When extrapolating the data points along lines of constant [VSLS]+$[\mathrm{Br_y^{inorg}}]$ bromine (grey dashed lines in Fig. 15) for SF1-2013, SF5-2013, and SF6-2013 to $[\mathrm{Br_y^{inorg}}] = 0$, and assuming no bromine is effectively lost in the troposphere, then the apparent concentrations of brominated VSLS at the surface should range between 4 - 8.5 ppt. However, frequently larger concentrations of brominated VSLS (some 10 ppt) are measured in boundary layer of the Pacific (e.g., Yokouchi et al. (1997), Schauffler et al. (1998), Wamsley et al. (1998) Yokouchi et al. (2005), Tegtmeier et al. (2012), Ashfold et al. (2012), Ziska et al. (2013), Sala et al. (2014), and others). Therefore effective loss processes for inorganic bromine, for example by heterogeneous uptake of inorganic bromine on aerosol and cloud particles, must act in the atmosphere.

Next, when subtracting from the given range (20.3 ppt to 22.3 ppt) of total $\mathrm{Br_y}$, the almost constant contribution of $\mathrm{CH_3Br}$ and the halons to total stratospheric bromine (14.6 ppt in 2013), a variable contribution from VSLS bromine (contribution 3), and $\mathrm{Br_y^{inorg}}$ (contribution 4) to total TTL bromine in the range of 5.7 ppt to 7.7 ppt (± 1.5 ppt) is calculated (Figure 15). We note that this range falls well into the range assessed in WMO (2014), or recently estimated by Navarro et al. (2015) (6 ppt range (4 - 9) ppt) for contribution of 3 and 4 to the total stratospheric $\mathrm{Br_y}$. It is, however, somewhat (up to 2 ppt) larger than some of the earlier studies, including our balloon-borne studies, indicated (for details see section 1).

Here one may wonder whether (a) this result is significant, or that (b) some $\mathrm{Br_y^{inorg}}$ is actually removed by heterogeneous processes in the TTL (e.g., Aschmann et al. (2011), Aschmann and Sinnhuber (2013), and others), or (c) that, TTL $\mathrm{Br_y}$ shows some seasonality analogous to the tape recorder for $\mathrm{H_2O}$ (e.g., Levine et al. (2008), Krüger et al. (2008), Fueglistaler et al. (2009), Schofield et al. (2011), Ploeger et al. (2011), and others).

Also remarkable are the the non-negligible amounts of $\mathrm{Br_y^{inorg}}$ (2.63 ± 1.04 ppt, range from 0.5 ppt to 5.25 ppt (which is from close to zero to 25% of all TTL bromine) inferred for altitudes at the bottom of the TTL (θ = 350 - 360 K), of which 40 to 50% may consist of BrO. This finding clearly sets a range and an upper limit for the $\mathrm{Br_y^{inorg}}$ influx into the TTL due to entrained air masses of recent tropospheric origin (contribution 4). Again, the latter can most likely be attributed to different source regions (and thus emission strengths) of the brominated VSLS, and a varying degree of photochemical processing of the air masses transported from the surface to the TTL. The increase in variance found for $\mathrm{Br_y^{inorg}}$, which increases in absolute terms, but decreases in relative terms (i.e. from 0.4 for θ in the range 350 K to 360 K to 0.3 for θ = 390 K to 400 K) with increasing θ is also noteworthy. This may indicate a subsequent flattening-out of the air-mass-to-air-mass variability of $\mathrm{Br_y^{inorg}}$ in aging air due to the photochemical decay of the brominated organic source gases and atmospheric mixing processes.

4.7 Implications for ozone

The ozone budget in the TOMCAT/SLIMCAT simulation has been analysed based on the rate-limiting steps of the catalytic ozone destruction cycles. The chemical rates are averaged over the tropical region (20°S - 20 °N) for the duration of the campaign. Within this domain, the net rate of ozone change varied from a loss of - 0.5 $\mathrm{ppbv/day}$ at the base of the TTL (θ = 355 K, p = 150 hPa) to a production of + 1.8 $\mathrm{ppbv/day}$ at the top (θ= 383 K, p = 90 hPa). This increase with height is due to the strong vertical gradient in the production rate of odd oxygen by $\mathrm{O_2}$ photolysis. Within the catalytic ozone loss cycles in the TTL, the model indicates that those containing bromine contribute between 8% (base of TTL) and 15% (top of TTL) of the total (not shown). By far the dominant contribution to this is through the cycle involving $\mathrm{BrO + HO_2}$ to form HOBr. Overall, the modeled ozone loss cycles which account for majority of the destruction in this region are those with the rate-limiting steps of the reaction $\mathrm{HO_2 + O_3}$ to form $\mathrm{OH + 2O_2}$ and the reaction of $\mathrm{HO_2 + HO_2}$ to form $\mathrm{H_2O_2}$, i.e. cycles involving $\mathrm{HO_x}$ species. Therefore, increases in the bromine loading of the TTL have the potential to deplete ozone, in a region where climate is most sensitive to $\mathrm{O_3}$ perturbations (Riese et al., 2012).

Quantifying the radiative impact of the $\mathrm{O_3}$ changes described above is the beyond the scope of this study. However, we can note that (i) recent work has highlighted the efficiency of brominated VSLS at influencing climate (through $\mathrm{O_3}$), owing to their efficient breakdown in the UTLS (Hossaini et al., 2015), and (ii) a significant increase in $\mathrm{Br_y}$ in this region (from VSLS or other sources) could be important for future climate forcing. The latter could conceivably occur given suggested climate-induced changes to tropospheric transport (e.g., Hossaini et al. (2012b)) and/or oxidizing capacity due to the expected increase in VSLS emissions from the rapidly growing aquaculture industry (WMO, 2014).

Atmos. Chem. Phys. Discuss., doi:10.5194/acp-2016-656, 2016
Manuscript under review for journal Atmos. Chem. Phys.
Published: 19 September 2016

5 Conclusions

The subtropical lowermost stratosphere, upper troposphere, and tropopause layer of the Eastern Pacific are probed for inorganic bromine during the convective season (February and March 2013). The measurements of CH_4, O_3, NO_2, BrO, and some organic brominated source gases are inter-compared with TOMCAT/SLIMCAT simulations. After the simulated TOMCAT/SLIMCAT curtains of O_3 are projected on the measured O_3 concentrations, measured and modeled CH_4 agree well. This agreement is not surprising, since O_3, and CH_4 are strongly correlated (see Fig. 10). This provides evidence that the relevant dynamical processes are represented well in the TOMCAT/SLIMCAT simulations. When the simulated curtains of NO_2 are adjusted with the same parameters as inferred above, excellent agreement is again found between measured and modeled NO_2, thus providing further confidence in our measurement technique, in the modeled NO_y photochemistry, and in our overall approach.

The measured and modeled TTL concentrations of CH_2Br_2, $CHBr_3$ are found to compare reasonably well after some adjustments to the surface concentrations and atmospheric life times of both species are applied to the model (e.g., $[CHBr_3]$ = 1.4 ppt, $[CH_2Br_2]$ = 1.05 ppt at the surface). Further, the contribution to bromine in the LS, UT, and TTL by some other VSLS chloro-bromo-hydrocabrons (e.g., Σ $[CHClBr_2, CHCl_2Br, CH_2ClBr, ...]$) is accounted for by assuming a constant surface concentration of 1 ppt in the model. From flight-to-flight total organic bromine inferred from these VSLS species is found to vary by ± 1 ppt in the TTL over the Eastern Pacific in early 2013, which clearly indicate different origins and possibly atmospheric processing of the investigated air masses.

The measured BrO concentrations range between 3 - 9 ppt in the subtropical LS. In the TTL they range between 0.5 ± 0.5 ppt at the bottom of the TTL, and about 5 ppt at θ = 400 K, in overall good agreement with the model simulations, and the expectation based on the decay of the brominated source gases, and atmospheric transport. In the TTL, the inferred Br_y^{inorg} is found to increase from a mean of 2.63 ± 1.04 ppt for θ in the range of 350 - 360 K to 5.11 ± 1.57 ppt for $\theta = 390 - 400$ K, respectively, whereas in the subtropical LS it reaches 7.66 ± 2.95 ppt for θ's in the range of 390 - 400 K. Also remarkable is the non-negligible Br_y^{inorg} found for the lowest altitudes of the TTL, i.e. 2.63 ± 1.04 ppt with a range from 0.5 ppt to 5.25 ppt (or close to zero percent up to 25% of all TTL bromine). This may indicate a sizable, but rather variable influx of inorganic bromine into the TTL, largely depending on the air mass history, i.e. source region, and atmospheric transport and processing.

Our findings on LS, and TTL Br_y^{inorg} are in broad agreement with past experimental and theoretical studies on the processes and amount of bromine injected by source gas and product gases into the TTL, and eventually into the extra-tropical lowermost stratosphere (Ko et al. (1997), Schauffler et al. (1998), Wamsley et al. (1998), Dvortsov et al. (1999), Pfeilsticker et al. (2000), Montzka et al. (2003), Salawitch (2006), Sinnhuber and Folkins (2006), Hendrick et al. (2007), Laube et al. (2008), Dorf et al. (2006b), Dorf et al. (2008), Sinnhuber et al. (2009), Salawitch et al. (2010), Schofield et al. (2011), Aschmann et al. (2011), Hossaini et al. (2012b), Ashfold et al. (2012), Hossaini et al. (2012a), Aschmann and Sinnhuber (2013), Sala et al. (2014), Wang et al. (2015), Liang et al. (2014), WMO (2014), Navarro et al. (2015), and many others). Our study, however, sets tighter limits than those previously existing on the amount of Br_y^{inorg} and Br_y^{org}, the influx of brominated source, and product gases, and the photochemistry of bromine in the TTL and LS.

In particular, our study (re-)emphasizes that (a) variable amounts of VSLS bromine and (b) non-negligible amounts of $\mathrm{Br_y^{inorg}}$ are also transported into the TTL. While process (a) may strongly depend on the source region and season (here: cite Hossaini 2016,acp-2015-822, when published), process (b) may depend on the efficiency of heterogeneous processing and removal of some $\mathrm{Br_y^{inorg}}$ by atmospheric (ice) clouds and aerosols (e.g., Aschmann et al. (2011), and Aschmann and Sinnhuber (2013)). Therefore it is not suprising that TTL $\mathrm{Br_y}$ is rather variable (i.e. 20.3 ppt to 22.3 ppt) in the studied season.

We also note that the amount of $\mathrm{Br_y}$ over the Eastern Pacific during the convective season assessed here and in the study of Navarro et al. (2015) is somewhat (up to 2 ppt) larger than that presently found on average in the stratosphere (e.g., Dorf et al. (2006b), Hendrick et al. (2007), Dorf et al. (2008), and WMO (2014)). By assuming that this gap is significant, additional processes may come into to the focus of stratospheric bromine research, i.e. the seasonality and possibly long-term trend of the bromine transported into the stratosphere (e.g., Levine et al. (2008), Krüger et al. (2008), Fueglistaler et al. (2009), Schofield et al. (2011), Ploeger et al. (2011), and others).

Conceivably adding some inorganic bromine (from contribution 4) to TTL bromine exerts an additional impact on ozone. Our model-based assessment led to a loss of - 0.5 ppbv/day at the base of the TTL (θ = 355 K), and a net production of + 1.8 ppbv/day at the top (θ = 383 K). Within the catalytic ozone loss cycles in the TTL, the model indicates that those containing bromine contribute between 8% (at the base of the TTL) and 15% (at the top of TTL) of the total.

Acknowledgements. This study was funded by through the NASA Upper Atmosphere Research Program (NASA ATTREX Grant numbers NNX10AO82A for HUPCRS, NNX10AO83A for GWAS, and NNX10AO80A for the mini-DOAS measurements). The NOAA ozone photometer and UCATS measurements were supported by the NASA ATTREX inter-agency agreement numbers NNA11AA54I and NNA11AA55I, respectively. Additional support for the mini-DOAS measurements came through the Deutsche ForschungsGemeinschaft, DFG (through grants PF-384 5-1/2, PF384 7-1/2 PF384 9-1/2, and PF384 12-1), and the EU project SHIVA (FP7-ENV-2007-1-226224). RuShan Gao, T. D. Thornberry, and D. W. Fahey were supported by the NOAA Atmospheric Composition and Climate Program, and the NASA Radiation Sciences Program. The TOMCAT/SLIMCAT modeling was supported by the NERC National Centre for Atmospheric Science (NCAS), UK and by the NERC TropHal project (NE/J02449X/1). We thank Dr. Eric Jensen (NASA Ames Research Center, Moffett Field, California) and his team for coordinating the NASA-ATTREX mission. We thank Joe McNorton for help with the NOAA and AGAGE $\mathrm{CH_4}$ data. E. Atlas and M. Navarro gratefully acknowledge R. Lueb, R. Hendershot and S. Gabbard for technical support in the field, and X. Zhu and L. Pope for GWAS data analysis. Jim Elkins of NOAA would like to acknowledge the assistance of G. S. Dutton, J. D. Nance, and B. D. Hall during the ATTREX flights, calibration, and integration.

References

Aschmann, J. and Sinnhuber, B.-M.: Contribution of very short-lived substances to stratospheric bromine loading: uncertainties and constraints, Atmospheric Chemistry and Physics, 13, 1203–1219, doi:10.5194/acp-13-1203-2013, http://www.atmos-chem-phys.net/13/1203/2013/, 2013.

Aschmann, J., Sinnhuber, B.-M., Atlas, E. L., and Schauffler, S. M.: Modeling the transport of very short-lived substances into the tropical upper troposphere and lower stratosphere, Atmospheric Chemistry and Physics, 9, 9237–9247, doi:10.5194/acp-9-9237-2009, http://www.atmos-chem-phys.net/9/9237/2009/, 2009.

Aschmann, J., Sinnhuber, B.-M., Chipperfield, M. P., and Hossaini, R.: Impact of deep convection and dehydration on bromine loading in the upper troposphere and lower stratosphere, Atmospheric Chemistry and Physics, 11, 2671–2687, doi:10.5194/acp-11-2671-2011, http://www.atmos-chem-phys.net/11/2671/2011/, 2011.

Ashfold, M. J., Harris, N. R. P., Atlas, E. L., Manning, A. J., and Pyle, J. A.: Transport of short-lived species into the Tropical Tropopause Layer, Atmospheric Chemistry and Physics, 12, 6309–6322, doi:10.5194/acp-12-6309-2012, http://www.atmos-chem-phys.net/12/6309/2012/, 2012.

Brinckmann, S., Engel, A., Bönisch, H., Quack, B., and Atlas, E.: Short-lived brominated hydrocarbons – observations in the source regions and the tropical tropopause layer, Atmospheric Chemistry and Physics, 12, 1213–1228, doi:10.5194/acp-12-1213-2012, http://www.atmos-chem-phys.net/12/1213/2012/, 2012.

Butz, A., Bösch, H., Camy-Peyret, C., Chipperfield, M. P., Dorf, M., Kreycy, S., Kritten, L., Prados-Roman, C., Schwärzle, J., and Pfeilsticker, K.: Constraints on inorganic gaseous iodine in the tropical upper troposphere and stratosphere inferred from balloon-borne solar occultation observations, Atmos. Chem. Phys., 9, 7229 – 7242, 2009.

Chen, H., Karion, A., Rella, C. W., Winderlich, J., Gerbig, C., Filges, A., Newberger, T., Sweeney, C., and Tans, P. P.: Accurate measurements of carbon monoxide in humid air using the cavity ring-down spectroscopy (CRDS) technique, Atmospheric Measurement Techniques, 6, 1031–1040, doi:10.5194/amt-6-1031-2013, http://www.atmos-meas-tech.net/6/1031/2013/, 2013.

Chipperfield, M., Dhomse, S., W. Feng, W., McKenzie, R., Velders, G., and Pyle, J.: Quantifying the ozone and ultraviolet benefits already achieved by the Montreal Protocol, Nature Communications, 6, doi:10.1029/96JD01167, 2015.

Chipperfield, M. P.: Multiannual simulations with a three-dimensional chemical transport model, J. Geophys. Res., 104, 1781–1805, 1999.

Chipperfield, M. P.: New Version of the TOMCAT/SLIMCAT Off-Line Chemical Transport Model: Intercomparison of Stratospheric Tracer Experiments, Q. J. Roy. Meteorol. Soc., 132, 1179–1203, doi:doi:10.1256/qj.05.51, 2006.

Crosson, E. R.: A cavity ring-down analyzer for measurements of atmospheric levels of methane, carbon dioxide, and water vapor, Appl. Phys. B, 92, 403 – 408, 2008.

Daniel, J. S., Schauffler, S. M., Pollock, W. H., Solomon, S., Weaver, A., Heidt, L. E., Garcia, R. R., Atlas, E. L., and Vedder, J. F.: On the age of stratospheric air and inorganic chlorine and bromine release, Journal of Geophysical Research: Atmospheres, 101, 16 757–16 770, doi:10.1029/96JD01167, http://dx.doi.org/10.1029/96JD01167, 1996.

Dee, D. P., Uppala, S. M., Simmons, A. J., Berrisford, P., Poli, P., Kobayashi, S., Andrae, U., Balmaseda, M. A., Balsamo, G., Bauer, P., Bechtold, P., Beljaars, A. C. M., van de Berg, L., Bidlot, J., Bormann, N., Delsol, C., Dragani, R., Fuentes, M., Geer, A. J., Haimberger, L., Healy, S. B., Hersbach, H., Hólm, E. V., Isaksen, L., Kallberg, P., Köhler, M., Matricardi, M., McNally, A. P., Monge-Sanz, B. M., Morcrette, J.-J., Park, B.-K., Peubey, C., de Rosnay, P., Tavolato, C., Thepaut, J.-N., and Vitart, F.: The ERA-Interim reanalysis:

configuration and performance of the data assimilation system, Quarterly Journal of the Royal Meteorological Society, 137, 553–597, doi:10.1002/qj.828, http://dx.doi.org/10.1002/qj.828, 2011.

Deutschmann, T., Beirle, S., Frieß, U., Grzegorski, M., Kern, C., Kritten, L., Platt, U., Pukite, J., Wagner, T., Werner, B., and Pfeilsticker, K.: The Monte Carlo Atmospheric Radiative Transfer Model McArtim: Introduction and Validation of Jacobians and 3D Features, Journal of Quantitative Spectroscopy and Radiative Transfer, 112, 1119–1137, 2011.

Dlugokencky, E. J., Myers, R. C., Lang, P. M., Masarie, K. A., Crotwell, A. M., Thoning, K. W., Hall, B. D., Elkins, J. W., and Steele, L. P.: Conversion of NOAA atmospheric dry air CH4 mole fractions to a gravimetrically prepared standard scale, Journal of Geophysical Research: Atmospheres, 110, n/a–n/a, doi:10.1029/2005JD006035, http://dx.doi.org/10.1029/2005JD006035, d18306, 2005.

Dorf, M., Bösch, H., Butz, A., Camy-Peyret, C., Chipperfield, M. P., Engel, A., Goutail, F., Grunow, K., Hendrick, F., Hrechanyy, S., Naujokat, B., Pommereau, J.-P., Van Roozendael, M., Sioris, C., Stroh, F., Weidner, F., and Pfeilsticker, K.: Balloon-borne stratospheric BrO measurements: comparison with Envisat/SCIAMACHY BrO limb profiles, Atmospheric Chemistry and Physics, 6, 2483–2501, doi:10.5194/acp-6-2483-2006, http://www.atmos-chem-phys.net/6/2483/2006/, 2006a.

Dorf, M., Butler, J. H., Butz, A., Camy-Peyret, C., Chipperfield, M. P., Kritten, L., Montzka, S. A., Simmes, B., Weidner, F., and Pfeilsticker, K.: Long-term observations of stratospheric bromine reveal slow down in growth, Geophysical Research Letters, 33, n/a–n/a, doi:10.1029/2006GL027714, http://dx.doi.org/10.1029/2006GL027714, 2006b.

Dorf, M., Butz, A., Camy-Peyret, C., Chipperfield, M. P., Kritten, L., and Pfeilsticker, K.: Bromine in the tropical troposphere and stratosphere as derived from balloon-borne BrO observations, Atmospheric Chemistry and Physics, 8, 7265–7271, doi:10.5194/acp-8-7265-2008, http://www.atmos-chem-phys.net/8/7265/2008/, 2008.

Dvortsov, V., Geller, M. A., Solomon, S., Schauffler, S. M., Atlas, E. L., and Blake, D. R.: Rethinking reactive halogen budget in the midlatitude stratosphere, Geophys. Res. Lett., 26, 1699–1702, 1999.

Elkins, J. W., Fahey, D. W., Gilligan, J. M., Dutton, G. S., Baring, T. J., Volk, C. M., Dunn, R. E., Myers, R. C., Montzka, S. A., Wamsley, P. R., Hayden, A. H., Butler, J. H., Thompson, T. M., Swanson, T. H., Dlugokencky, E. J., Novelli, P. C., Hurst, D. F., Lobert, J. M., Ciciora, S. J., McLaughlin, R. J., Thompson, T. L., Winkler, R. H., Fraser, P. J., Steele, L. P., and Lucarelli, M. P.: Airborne gas chromatograph for in situ measurements of long-lived species in the upper troposphere and lower stratosphere, Geophysical Research Letters, 23, 347 – 350, doi:10.1029/96GL00244, http://dx.doi.org/10.1029/96GL00244, 1996.

Feng, W., Chipperfield, M. P., Dhomse, S., Monge-Sanz, B. M., Yang, X., Zhang, K., and Ramonet, M.: Evaluation of cloud convection and tracer transport in a three-dimensional chemical transport model, Atmospheric Chemistry and Physics, 11, 5783–5803, doi:10.5194/acp-11-5783-2011, http://www.atmos-chem-phys.net/11/5783/2011/, 2011.

Fernandez, R. P., Salawitch, R. J., Kinnison, D. E., Lamarque, J.-F., and Saiz-Lopez, A.: Bromine partitioning in the tropical tropopause layer: implications for stratospheric injection, Atmospheric Chemistry and Physics, 14, 13 391–13 410, doi:10.5194/acp-14-13391-2014, http://www.atmos-chem-phys.net/14/13391/2014/, 2014.

Fitzenberger, R., Bösch, H., Camy-Peyret, C., Chpperfield, M., Harder, H., Platt, U., Pyle, J., Wagner, T., and Pfeilsticker, K.: First profile measurement of tropospheric BrO, Geophys. Res. Lett., 27, 2921–2924, 2000.

Fueglistaler, S., Dessler, A. E., Dunkerton, T. J., Folkins, I., Fu, Q., and Mote, P. W.: Tropical tropopause layer, Reviews of Geophysics, 47, n/a–n/a, doi:10.1029/2008RG000267, http://dx.doi.org/10.1029/2008RG000267, 2009.

Gao, R. S., Ballard, J., Watts, L. A., Thornberry, T. D., Ciciora, S. J., McLaughlin, R. J., and Fahey, D. W.: A compact, fast UV photometer for measurement of ozone from research aircraft, Atmospheric Measurement Techniques, 5, 2201–2210, doi:10.5194/amt-5-2201-2012, http://www.atmos-meas-tech.net/5/2201/2012/, 2012.

Harder, H., Bösch, H., Camy-Peyret, C., Chipperfield, M. P., Fitzenberger, R., Payan, S., Perner, D., Platt, U., Sinnhuber, B.-M., and Pfeilsticker, K.: Comparison of measured and modeled stratospheric BrO: Implications for the total amount of stratospheric bromine, Geophysical Research Letters, 27, 3695–3698, doi:10.1029/1999GL011215, http://dx.doi.org/10.1029/1999GL011215, 2000.

Heidt, L. E., Vedder, J. F., Pollock, W. H., Lueb, R. A., and Henry, B. E.: Trace gases in the Antarctic atmosphere, Journal of Geophysical Research: Atmospheres, 94, 11 599–11 611, doi:10.1029/JD094iD09p11599, http://dx.doi.org/10.1029/JD094iD09p11599, 1989.

Hendrick, F., Van Roozendael, M., Chipperfield, M. P., Dorf, M., Goutail, F., Yang, X., Fayt, C., Hermans, C., Pfeilsticker, K., Pommereau, J.-P., Pyle, J. A., Theys, N., and De Mazière, M.: Retrieval of stratospheric and tropospheric BrO profiles and columns using ground-based zenith-sky DOAS observations at Harestua, 60^o N, Atmospheric Chemistry and Physics, 7, 4869–4885, doi:10.5194/acp-7-4869-2007, http://www.atmos-chem-phys.net/7/4869/2007/, 2007.

Hossaini, R., Chipperfield, M. P., Dhomse, S., Ordóñez, C., Saiz-Lopez, A., Abraham, N. L., Archibald, A., Braesicke, P., Telford, P., Warwick, N., Yang, X., and Pyle, J.: Modelling future changes to the stratospheric source gas injection of biogenic bromocarbons, Geophysical Research Letters, 39, n/a–n/a, doi:10.1029/2012GL053401, http://dx.doi.org/10.1029/2012GL053401, l20813, 2012a.

Hossaini, R., Chipperfield, M. P., Feng, W., Breider, T. J., Atlas, E., Montzka, S. A., Miller, B. R., Moore, F., and Elkins, J.: The contribution of natural and anthropogenic very short-lived species to stratospheric bromine, Atmospheric Chemistry and Physics, 12, 371–380, doi:10.5194/acp-12-371-2012, http://www.atmos-chem-phys.net/12/371/2012/, 2012b.

Hossaini, R., Mantle, H., Chipperfield, M. P., Montzka, S. A., Hamer, P., Ziska, F., Quack, B., Krüger, K., Tegtmeier, S., Atlas, E., Sala, S., Engel, A., Bönisch, H., Keber, T., Oram, D., Mills, G., Ordóñez, C., Saiz-Lopez, A., Warwick, N., Liang, Q., Feng, W., Moore, F., Miller, B. R., Marécal, V., Richards, N. A. D., Dorf, M., and Pfeilsticker, K.: Evaluating global emission inventories of biogenic bromocarbons, Atmospheric Chemistry and Physics, 13, 11 819–11 838, doi:10.5194/acp-13-11819-2013, http://www.atmos-chem-phys.net/13/11819/2013/, 2013.

Hossaini, R., Chipperfield, M. P. and. Montzka, S. A., Rap, A., Dhomse, S., and Feng, W.: Efficiency of short-lived halogens at influencing climate through depletion of stratospheric ozone, Nature Geoscience, 8, 186 – 190, doi:doi:10.1038/ngeo2363, http://www.nature.com/ngeo/journal/vaop/ncurrent/full/ngeo2363.html, 2015.

Jensen, E.-J., Pfister, L., Jordan, D. E., Fahey, D. W., Newman, P. A., Thornberry, T., Rollins, A., Diskin, G., Bui, T. P., McGill, M., Hlavka, D., Lawson, R. P., Gao, R.-S., Pilewskie, P., Elkins, J., Hintsa, E., Moore, F., Mahoney, M. J., Atlas, E., Stutz, J., Pfeilsticker, K., Wofsy, S., Evan, S., and Rosenlof, K. H.: The NASA Airborne Tropical TRopopause EXperiment (ATTREX), SPARC newsletter, 41, 15 – 24, http://issuu.com/sparc-climate/docs/41_sparcnewsletter_jul2013_web/24, 2013.

Jensen, E. J., Pfister, L., Jordan, D. E., Bui, T. V., Ueyama, R., Singh, H. B., Thornberry, T., Rollins, A. W., Gao, R.-S., Fahey, D. W., Rosenlof, K. H., Elkins, J. W., Diskin, G. S., DiGangi, J. P., Lawson, R. P., Woods, S., Atlas, E. L., Rodriguez, M. A. N., Wofsy, S. C., Pittman, J., Bardeen, C. G., Toon, O. B., Kindel, B. C., Newman, P. A., McGill, M. J., Hlavka, D. L., Lait, L. R., Schoeberl, M. R., Bergman, J. W., Selkirk, H. B., Alexander, M. J., Kim, J.-E., Lim, B. H., Stutz, J., and Pfeilsticker, K.: The NASA Airborne Tropical TRopopause EXperiment (ATTREX): High-Altitude Aircraft Measurements in the Tropical Western Pacific, Bulletin of the American Meteorological Society, 0, null, doi:10.1175/BAMS-D-14-00263.1, http://dx.doi.org/10.1175/BAMS-D-14-00263.1, 2015.

Ko, M., Sze, N., Scott, C., and Weisenstein, D.: On the relation between chlorine/bromine loading and short-lived tropospheric source gases, J. Geophys. Res., 102, 25,507 – 25,517, 1997.

Ko, M. K. W., Newman, P. A., Reimann, S., and Strahan, E.: Lifetimes of Stratospheric Ozone-Depleting Substances, Their Replacements, and Related Species, SPARC Report, WCRP-15/2013, 1 – 255, 2013.

Kreycy, S., Camy-Peyret, C., Chipperfield, M. P., Dorf, M., Feng, W., Hossaini, R., Kritten, L., Werner, B., and Pfeilsticker, K.: Atmospheric test of the $\mathrm{J(BrONO_2)/k_{BrO+NO_2}}$ ratio: implications for total stratospheric Br_y and bromine-mediated ozone loss, Atmospheric Chemistry and Physics, 13, 6263–6274, doi:10.5194/acp-13-6263-2013, http://www.atmos-chem-phys.net/13/6263/2013/, 2013.

Kritten, L., Butz, A., Dorf, M., Deutschmann, T., Kühl, S., Prados-Roman, C., Pukite, J., Rozanov, A., Schofield, R., and Pfeilsticker, K.: Balloon-borne limb measurements of the diurnal variation of UV/vis absorbing radicals – a case study on NO_2 and O_3, Atmos. Meas. Techn., 3, 933 – 946, 2010.

Kritten, L., Butz, A., Chipperfield, M. P., Dorf, M., Dhomse, S., Hossaini, R., Oelhaf, H., Prados-Roman, C., Wetzel, G., and Pfeilsticker, K.: Constraining the N_2O_5 UV absorption cross section from spectroscopic trace gas measurements in the tropical mid-stratosphere, Atmospheric Chemistry and Physics, 14, 9555–9566, doi:10.5194/acp-14-9555-2014, http://www.atmos-chem-phys.net/14/9555/2014/, 2014.

Krüger, K., Tegtmeier, S., and Rex, M.: Long-term climatology of air mass transport through the Tropical Tropopause Layer (TTL) during NH winter, Atmospheric Chemistry and Physics, 8, 813–823, doi:10.5194/acp-8-813-2008, http://www.atmos-chem-phys.net/8/813/2008/, 2008.

Laube, J. C., Engel, A., Bönisch, H., Möbius, T., Worton, D. R., Sturges, W. T., Grunow, K., and Schmidt, U.: Contribution of very short-lived organic substances to stratospheric chlorine and bromine in the tropics – a case study, Atmospheric Chemistry and Physics, 8, 7325–7334, doi:10.5194/acp-8-7325-2008, http://www.atmos-chem-phys.net/8/7325/2008/, 2008.

Levine, J. G., Braesicke, P., Harris, N. R. P., and Pyle, J. A.: Seasonal and inter-annual variations in troposphere-to-stratosphere transport from the tropical tropopause layer, Atmospheric Chemistry and Physics, 8, 3689 – 3703, doi:10.5194/acp-8-3689-2008, http://www.atmos-chem-phys.net/8/3689/2008/, 2008.

Liang, Q., Atlas, E., Blake, D., Dorf, M., Pfeilsticker, K., and Schauffler, S.: Convective transport of very short lived bromocarbons to the stratosphere, Atmospheric Chemistry and Physics, 14, 5781–5792, doi:10.5194/acp-14-5781-2014, http://www.atmos-chem-phys.net/14/5781/2014/, 2014.

Mellouki, A., Talukdar, R. K., Schmoltner, A.-M., Gierczak, T., Mills, M. J., Solomon, S., and Ravishankara, A. R.: Atmospheric lifetimes and ozone depletion potentials of methyl bromide (CH_3Br) and dibromomethane (CH_2Br_2), Geophys. Res. Lett., 19, 2059 – 2062, 1992.

Michael, J. V., Lee, J. H., Payne, W. A., and Stief, L. J.: Absolute rate of reaction of bromine atoms with ozone from 200 - 360 K, J. Atmos. Chem., 68, 4093 – 4097, 1978.

Michelsen, H. A., Manney, G. L., Gunson, M. R., Rinsland, C. P., and Zander, R.: Correlations of stratospheric abundances of CH4 and N2O derived from ATMOS measurements, Geophysical Research Letters, 25, 2777–2780, doi:10.1029/98GL01977, http://dx.doi.org/10.1029/98GL01977, 1998.

Montzka, S., Butler, J., Hall, B., Mondell, D., and Elkins, J.: A decline in tropospheric organic bromine, Geophys. Res. Lett., 30, 1826–1829, 2003.

Moore, F. L., Elkins, J. W., Ray, E. A., Dutton, G. S., Dunn, R. E., Fahey, D. W., McLaughlin, R. J., Thompson, T. L., Romashkin, P. A., Hurst, D. F., and Wamsley, P. R.: Balloonborne in situ gas chromatograph for measurements in the troposphere and stratosphere, Journal of Geophysical Research: Atmospheres, 108, n/a–n/a, doi:10.1029/2001JD000891, http://dx.doi.org/10.1029/2001JD000891, 8330, 2003.

Navarro, M. A., Atlas, E. L., Saiz-Lopez, A., Rodriguez-Lloveras, X., Kinnison, D. E., Lamarque, J.-F., Tilmes, S., Filus, M., Harris, N. R. P., Meneguz, E., Ashfold, M. J., Manning, A. J., Cuevas, C. A., Schauffler, S. M., and Donets, V.: Airborne measurements of organic bromine compounds in the Pacific tropical tropopause layer, Proceedings of the National Academy of Sciences, 112, 13 789–13 793, doi:10.1073/pnas.1511463112, http://www.pnas.org/content/112/45/13789.abstract, 2015.

Nicovich, J. M., Kreutter, K. D., and Wine, P. H.: Kinetics of the Reactions of Cl(^2P_j) and Br($^2P_{3/2}$) with O_3, Int. J. Chem. Kinet., 22, 399 –414, 1990.

Orbe, C., Waugh, D. W., and Newman, P. A.: Air-mass origin in the tropical lower stratosphere: The influence of Asian boundary layer air, Geophysical Research Letters, 42, 4240–4248, doi:10.1002/2015GL063937, http://dx.doi.org/10.1002/2015GL063937, 2015GL063937, 2015.

Parrella, J. P., Chance, K., Salawitch, R. J., Canty, T., Dorf, M., and Pfeilsticker, K.: New retrieval of BrO from SCIAMACHY limb: an estimate of the stratospheric bromine loading during April 2008, Atmospheric Measurement Techniques, 6, 2549–2561, doi:10.5194/amt-6-2549-2013, http://www.atmos-meas-tech.net/6/2549/2013/, 2013.

Pfeilsticker, K., Sturges, W. T., Bösch, H., Camy-Peyret, C., Chipperfield, M. P., Engel, A., Fitzenberger, R., Müller, M., Payan, S., and Sinnhuber, B.-M.: Lower stratospheric organic and inorganic bromine budget for the Arctic winter 1998/99, Geophysical Research Letters, 27, 3305–3308, doi:10.1029/2000GL011650, http://dx.doi.org/10.1029/2000GL011650, 2000.

Platt, U. and Stutz, J.: Differential Optical Absorption Spectroscopy (DOAS), Principle and Applications, ISBN 3-340-21193-4, Springer Verlag, Heidelberg, 2008.

Ploeger, F., Fueglistaler, S., Grooß, J.-U., Günther, G., Konopka, P., Liu, Y., Müller, R., Ravegnani, F., Schiller, C., Ulanovski, A., and Riese, M.: Insight from ozone and water vapour on transport in the tropical tropopause layer (TTL), Atmospheric Chemistry and Physics, 11, 407–419, doi:10.5194/acp-11-407-2011, http://www.atmos-chem-phys.net/11/407/2011/, 2011.

Proffitt, M. H. and McLaughlin, R. J.: Fast-response dual-beam UV-absorption ozone photometer suitable for use on stratospheric balloons, Rev. Sci. Instrum., 54, 1719 – 1728, 1983.

Raecke, R.: Atmospheric spectoscopy of trace gases and water vapour in the tropical tropopause layer from the NASA Global Hawk, Master thesis, Institut für Umweltphysik, Universität Heidelberg, 2013.

Ravishankara, A. R., , Daniel, J., and W., P. R.: Nitrous Oxide (N_2O): The Dominant Ozone-Depleting Substance Emitted in the 21st Century, Science, 326, 123–125, 2009.

Rella, C. W., Chen, H., Andrews, A. E., Filges, A., Gerbig, C., Hatakka, J., Karion, A., Miles, N. L., Richardson, S. J., Steinbacher, M., Sweeney, C., Wastine, B., and Zellweger, C.: High accuracy measurements of dry mole fractions of carbon dioxide and methane in humid air, Atmospheric Measurement Techniques, 6, 837–860, doi:10.5194/amt-6-837-2013, http://www.atmos-meas-tech.net/6/837/2013/, 2013.

Richter, A., Wittrock, F., Ladstätter-Weiß enmayer, A., and Burrows, J.: GOME measurements of stratospheric and tropospheric BrO, Adv. Space Res.,, 29, 1667–1672, doi:doi:10.1016/S0273-1177(02)00123-0, 2002.

Riese, M., Ploeger, F., Rap, A., Vogel, B., Konopka, P., Dameris, M., and Forster, P.: Impact of uncertainties in atmospheric mixing on simulated UTLS composition and related radiative effects, Journal of Geophysical Research: Atmospheres, 117, n/a–n/a, doi:10.1029/2012JD017751, http://dx.doi.org/10.1029/2012JD017751, d16305, 2012.

Rodgers, C.: Inverse methods for atmospheric sounding, World Scientific, Singapore, New Jersey, London, Hongkong, 2000.

Rozanov, A., Kühl, S., Doicu, A., McLinden, C., Pukite, J., Bovensmann, H., Burrows, J. P., Deutschmann, T., Dorf, M., Goutail, F., Grunow, K., Hendrick, F., von Hobe, M., Hrechanyy, S., Lichtenberg, G., Pfeilsticker, K., Pommereau, J. P., Van Roozendael, M., Stroh, F., and Wagner, T.: BrO vertical distributions from SCIAMACHY limb measurements: comparison of algorithms and retrieval results, Atmospheric Measurement Techniques, 4, 1319–1359, doi:10.5194/amt-4-1319-2011, http://www.atmos-meas-tech.net/4/1319/2011/, 2011.

Saiz-Lopez, A. and Fernandez, R. P.: On the formation of tropical rings of atomic halogens: Causes and implications, Geophysical Research Letters, pp. n/a–n/a, doi:10.1002/2015GL067608, http://dx.doi.org/10.1002/2015GL067608, 2015GL067608, 2016.

Sala, S., Bönisch, H., Keber, T., Oram, D. E., Mills, G., and Engel, A.: Deriving an atmospheric budget of total organic bromine using airborne in situ measurements from the western Pacific area during SHIVA, Atmospheric Chemistry and Physics, 14, 6903–6923, doi:10.5194/acp-14-6903-2014, http://www.atmos-chem-phys.net/14/6903/2014/, 2014.

Salawitch, R.: Atmospheric chemistry: Biogenic bromine, Nature, 439, 275 – 277, 2006.

Salawitch, R. J., Canty, T., Kurosu, T., Chance, K., Liang, Q., da Silva, A., Pawson, S., Nielsen, J. E., Rodriguez, J. M., Bhartia, P. K., Liu, X., Huey, L. G., Liao, J., Stickel, R. E., Tanner, D. J., Dibb, J. E., Simpson, W. R., Donohoue, D., Weinheimer, A., Flocke, F., Knapp, D., Montzka, D., Neuman, J. A., Nowak, J. B., Ryerson, T. B., Oltmans, S., Blake, D. R., Atlas, E. L., Kinnison, D. E., Tilmes, S., Pan, L. L., Hendrick, F., Van Roozendael, M., Kreher, K., Johnston, P. V., Gao, R. S., Johnson, B., Bui, T. P., Chen, G., Pierce, R. B., Crawford, J. H., and Jacob, D. J.: A new interpretation of total column BrO during Arctic spring, Geophysical Research Letters, 37, n/a–n/a, doi:10.1029/2010GL043798, http://dx.doi.org/10.1029/2010GL043798, l21805, 2010.

Sander, S., Friedl, R. R., Barkern, J., Golden, D., Kurylo, M., Wine, P., Abbat, J., Burkholder, J., Moortgaret, C., Huie, R., and Orkin, R. E.: Chemical kinetics and photochemical data for use in atmospheric studies, Technical Report, NASA/JPL Publication, 17, 2011.

Schauffler, S., Atlas, E., Blake, D., Flocke, F., Lueb, R., Lee-Taylor, J., Stroud, V., , and Travnicek, W.: Distribution of brominated organic compounds in the upper troposphere and lower stratosphere, J. Geophys. Res., 104, 21,513–21,535, 1999.

Schauffler, S. M., Heidt, L. E., Pollock, W. H., Gilpin, T. M., Vedder, J. F., Solomon, S., Lueb, R. A., and Atlas, E. L.: Measurements of halogenated organic compounds near the tropical tropopause, Geophysical Research Letters, 20, 2567–2570, doi:10.1029/93GL02840, http://dx.doi.org/10.1029/93GL02840, 1993.

Schauffler, S. M., Atlas, E. L., Flocke, F., Lueb, R. A., Stroud, V., and Travnicek, W.: Measurement of bromine-containing organic compounds at the tropical tropopause, Geophys. Res. Lett., 25, 317–320, 1998.

Schofield, R., <, S., Wohltmann, I., and Rex, M.: Sensitivity of stratospheric Br_y to uncertainties in very short lived substance emissions and atmospheric transport, Atmospheric Chemistry and Physics, 11, 1379–1392, doi:10.5194/acp-11-1379-2011, http://www.atmos-chem-phys.net/11/1379/2011/, 2011.

Sinnhuber, B.-M. and Folkins, I.: Estimating the contribution of bromoform to stratospheric bromine and its relation to dehydration in the tropical tropopause layer, Atmospheric Chemistry and Physics, 6, 4755–4761, doi:10.5194/acp-6-4755-2006, http://www.atmos-chem-phys.net/6/4755/2006/, 2006.

Sinnhuber, B.-M., Sheode, N., Chipperfield, M. P., and Feng, W.: The contribution of anthropogenic bromine emissions to past stratospheric ozone trends: a modelling study, Atmos. Chem. Phys., 9, 2863–2871, 2009.

Sioris, C. E., Kovalenko, L. J., McLinden, C. A., Salawitch, R. J., Van Roozendael, M., Goutail, F., Dorf, M., Pfeilsticker, K., Chance, K., von Savigny, C., Liu, X., Kurosu, T. P., Pommereau, J.-P., Bösch, H., and Frerick, J.: Latitudinal and vertical distribution of bromine monoxide in the lower stratosphere from Scanning Imaging Absorption Spectrometer for Atmospheric Chartography limb scattering measurements, Journal of Geophysical Research: Atmospheres, 111, n/a–n/a, doi:10.1029/2005JD006479, http://dx.doi.org/10.1029/2005JD006479, 2006.

Stachnik, R. A., Millán, L., Jarnot, R., Monroe, R., McLinden, C., Kühl, S., Pukite, J., Shiotani, M., Suzuki, M., Kasai, Y., Goutail, F., Pommereau, J. P., Dorf, M., and Pfeilsticker, K.: Stratospheric BrO abundance measured by a balloon-borne submillimeterwave radiometer, Atmospheric Chemistry and Physics, 13, 3307–3319, doi:10.5194/acp-13-3307-2013, http://www.atmos-chem-phys.net/13/3307/2013/, 2013.

Sturges, W. T., Oram, D. E., Carpenter, L. J., Penkett, S. A., and Engel, A.: Bromoform as a source of stratospheric bromine, Geophysical Research Letters, 27, 2081–2084, doi:10.1029/2000GL011444, http://dx.doi.org/10.1029/2000GL011444, 2000.

Stutz, J., Werner, B., Spolaor, M., Scalone, L., Festa, J., Tsai, C., Cheung, R., Colosimo, S. F., Tricoli, U., Raecke, R., Gao, R.-S., Hintsa, E. J., Elkins, J. W., Moore, F. L., Hossaini, R., Feng, W., Chipperfield, M. P., Daube, B., Pittman, J., Wofsy, S., and Pfeilsticker, K.: A New Differential Optical Absorption Spectroscopy Instrument to Study Atmospheric Chemistry from an High-Altitude Unmanned Aircraft, Atmospheric Measurement Techniques Discussions, amt-2016-251, 2016.

Tegtmeier, S., Krüger, K., Quack, B., Atlas, E. L., Pisso, I., Stohl, A., and Yang, X.: Emission and transport of bromocarbons: from the West Pacific ocean into the stratosphere, Atmospheric Chemistry and Physics, 12, 10 633–10 648, doi:10.5194/acp-12-10633-2012, http://www.atmos-chem-phys.net/12/10633/2012/, 2012.

Theys, N., Van Roozendael, M., Errera, Q., Hendrick, F., Daerden, F., Chabrillat, S., Dorf, M., Pfeilsticker, K., Rozanov, A., Lotz, W., Burrows, J. P., Lambert, J.-C., Goutail, F., Roscoe, H. K., and De Mazière, M.: A global stratospheric bromine monoxide climatology based on the BASCOE chemical transport model, Atmospheric Chemistry and Physics, 9, 831–848, doi:10.5194/acp-9-831-2009, http://www.atmos-chem-phys.net/9/831/2009/, 2009.

Theys, N., Van Roozendael, M., Hendrick, F., Yang, X., De Smedt, I., Richter, A., Begoin, M., Errera, Q., Johnston, P. V., Kreher, K., and De Mazière, M.: Global observations of tropospheric BrO columns using GOME-2 satellite data, Atmospheric Chemistry and Physics, 11, 1791–1811, doi:10.5194/acp-11-1791-2011, http://www.atmos-chem-phys.net/11/1791/2011/, 2011.

Van Roozendael, M., Wagner, T., Richter, A., Pundt, I., Arlander, D., Burrows, J., Chipperfield, M. P., Fayt, C., Johnston, P., Lambert, J., Kreher, K., Pfeilsticker, K., Platt, U., Pommereau, J. P., Sinnhuber, B., Tornkvist, K., and Wittrock, F.: Intercomparison of BrO Measurements from ERS-2 GOME, Ground-based and balloon platforms, Adv. Space. Res., 29, 1161 – 1666, 2002.

Volkamer, R., Baidar, S., Campos, T. L., Coburn, S., DiGangi, J. P., Dix, B., Eloranta, E. W., Koenig, T. K., Morley, B., Ortega, I., Pierce, B. R., Reeves, M., Sinreich, R., Wang, S., Zondlo, M. A., and Romashkin, P. A.: Aircraft measurements of BrO, IO, glyoxal, NO_2, H_2O, O_2–O_2 and aerosol extinction profiles in the tropics: comparison with aircraft-/ship-based in situ and lidar measurements, Atmospheric Measurement Techniques, 8, 2121–2148, doi:10.5194/amt-8-2121-2015, http://www.atmos-meas-tech.net/8/2121/2015/, 2015.

Wamsley, P. R., Elkins, J. W., Fahey, D. W., Dutton, G. S., Volk, C. M. Myers, R. C., Montzka, S. A., Butler, J. H., Clarke, A. D., Fraser, P. J., Steele, L. P., Lucarelli, M. P., Atlas, E. L., Schauffler, S. M., Blake, D. R., Rowland, F. S., Sturges, W. T., Lee, J. M., Penkett, S. A., Engel, A., Stimpfle, R. M., Chan, K. R., Weisenstein, D. K., Ko, M. K. W., and Salawitch, R. J.: Distribution of halon-1211 in the upper troposphere and lower stratosphere and the 1994 total bromine budget, J. Geophys. Res, 103, 1513–1526, 1998.

Wang, S., Schmidt, J. A., Baidar, S., Coburn, S., Dix, B., Koenig, T. K., Apel, E., Bowdalo, D., Campos, T. L., Eloranta, E., Evans, M. J., DiGangi, J. P., Zondlo, M. A., Gao, R.-S., Haggerty, J. A., Hall, S. R., Hornbrook, R. S., Jacob, D., Morley, B., Pierce, B., Reeves, M., Romashkin, P., ter Schure, A., and Volkamer, R.: Active and widespread halogen chemistry in the tropical and subtropical free troposphere, Proceedings of the National Academy of Sciences, 112, 9281–9286, doi:10.1073/pnas.1505142112, http://www.pnas.org/content/112/30/9281.abstract, 2015.

Weidner, F., Bösch, H., Bovensmann, H., Burrows, J. P., Butz, A., Camy-Peyret, C., Dorf, M., Gerilowski, K., Gurlit, W., Platt, U., von Friedeburg, C., Wagner, T., and Pfeilsticker, K.: Balloon-borne limb profiling of UV/vis skylight radiances, O_3, NO_2, and BrO: technical set-up and validation of the method, Atmospheric Chemistry and Physics, 5, 1409–1422, doi:10.5194/acp-5-1409-2005, http://www.atmos-chem-phys.net/5/1409/2005/, 2005.

Wisher, A., Oram, D. E., Laube, J. C., Mills, G. P., van Velthoven, P., Zahn, A., and Brenninkmeijer, C. A. M.: Very short-lived bromomethanes measured by the CARIBIC observatory over the North Atlantic, Africa and Southeast Asia during 2009 - 2013, Atmospheric Chemistry and Physics, 14, 3557 – 3570, doi:10.5194/acp-14-3557-2014, http://www.atmos-chem-phys.net/14/3557/2014/, 2014.

WMO: Scientific assessment of ozone depletion: 2014, World Meteorological Organisation (WMO), Geneve, Switzerland, 55, 416pp, 2014.

Wofsy, S. C., Daube, B., Jimenez, R., Kort, E., Pittman, J., Park, S., Commane, R., Xiang, B., Santoni, G. ans Jacob, D., Fisher, J., Pickett-Heaps, C., Wang, H., Wecht, K., Wang, Q.-Q., Stephens, B., Shertz, S., Romashkin, P., Campos, T., Haggerty, J., Cooper, W., Rogers, D., Beaton, S., Hendershot, R., Elkins, J. W., Fahey, D. W., Gao, F. R. S., Moore, F., Montzka, S. A., Schwarz, D. J. P., Miller, Hurst, B., Sweeney, C., Oltmans, S. J., Nance, D., Hintsa, E., Dutton, G., Watts, L. A., Spackman, J. R., Rosenlof, K. H., Ray, E. A., Zondlo, M., Diao, M., Keeling, R., Bent, J., Atlas, E., Lueb, R., Mahoney, M., Chahine, M., Olson, E., Patra, P., Ishijima, K., Engelen, R., Flemming, J., Nassar, R., D.B.A., J., and M., F. S.: HIAPER Pole-to-Pole Observations (HIPPO): fine-grained, global-scale measurements of climatically important atmospheric gases and aerosols, Philosophical Transactions of the Royal Society of London A: Mathematical, Physical and Engineering Sciences, 369, 2073–2086, doi:10.1098/rsta.2010.0313, 2011.

Yokouchi, Y., Mukai, H., Yamamoto, H., Otsuki, A., Saitoh, C., and Nojiri, Y.: Distribution of methyl iodide, ethyl iodide, bromoform, and dibromomethane over the ocean (east and southeast Asian seas and the western Pacific), J. Geophys. Res., 102, 8805–8809, 1997.

Yokouchi, Y., Hasebe, F., Fujiwara, M., Takashima, H., Shiotani, M., Nishi, N., Kanaya, Y., Hashimoto, S., Fraser, P., Toom-Sauntry, D., Mukai, H., and Nojiri, Y.: Correlations and emission ratios among bromoform, dibromochloromethane, and dibromomethane in the atmosphere, Journal of Geophysical Research: Atmospheres, 110, n/a–n/a, doi:10.1029/2005JD006303, http://dx.doi.org/10.1029/2005JD006303, d23309, 2005.

Ziska, F., Quack, B., Abrahamsson, K., Archer, S. D., Atlas, E., Bell, T., Butler, J. H., Carpenter, L. J., Jones, C. E., Harris, N. R. P., Hepach, H., Heumann, K. G., Hughes, C., Kuss, J., Krüger, K., Liss, P., Moore, R. M., Orlikowska, A., Raimund, S., Reeves, C. E., Reifenhäuser, W., Robinson, A. D., Schall, C., Tanhua, T., Tegtmeier, S., Turner, S., Wang, L., Wallace, D., Williams, J., Yamamoto, H., Yvon-Lewis, S., and Yokouchi, Y.: Global sea-to-air flux climatology for bromoform, dibromomethane and methyl iodide, Atmospheric Chemistry and Physics, 13, 8915–8934, doi:10.5194/acp-13-8915-2013, http://www.atmos-chem-phys.net/13/8915/2013/, 2013.

Atmos. Chem. Phys. Discuss., doi:10.5194/acp-2016-656, 2016
Manuscript under review for journal Atmos. Chem. Phys.
Published: 19 September 2016

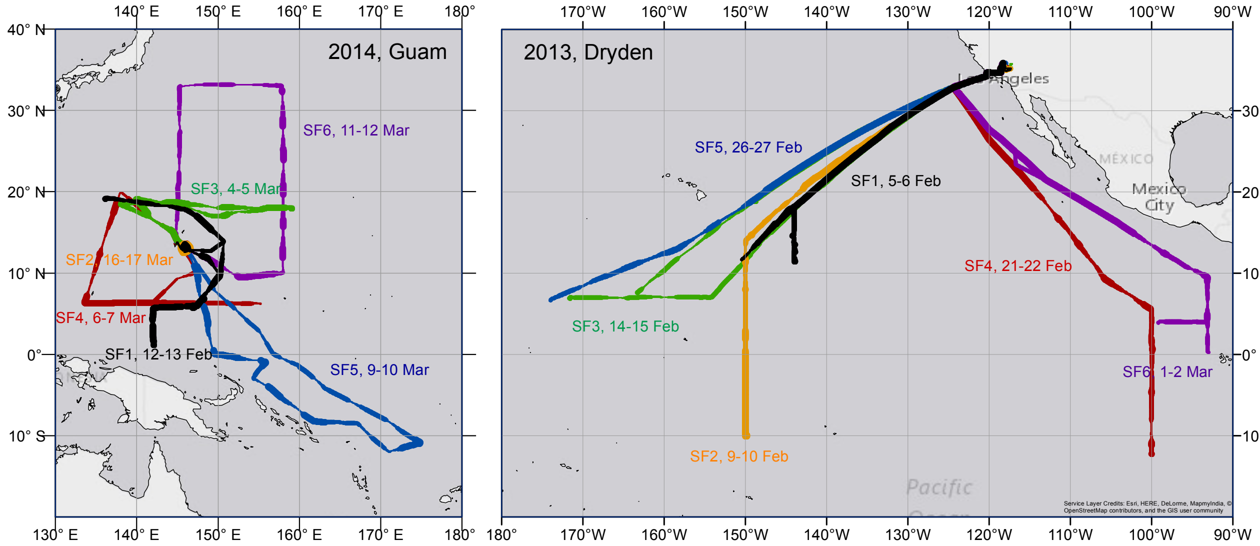

Figure 1. Overview of the NASA Global Hawk ATTREX flights; for (left) the Guam 2014 campaign and (right) the Edwards Air Force base (EAFB) 2013 campaign. The thickness of lines correspond to flight altitudes, where the thinnest line is for an altitude of around 14 km and the thickest line for around 18 km.

Atmos. Chem. Phys. Discuss., doi:10.5194/acp-2016-656, 2016
Manuscript under review for journal Atmos. Chem. Phys.
Published: 19 September 2016

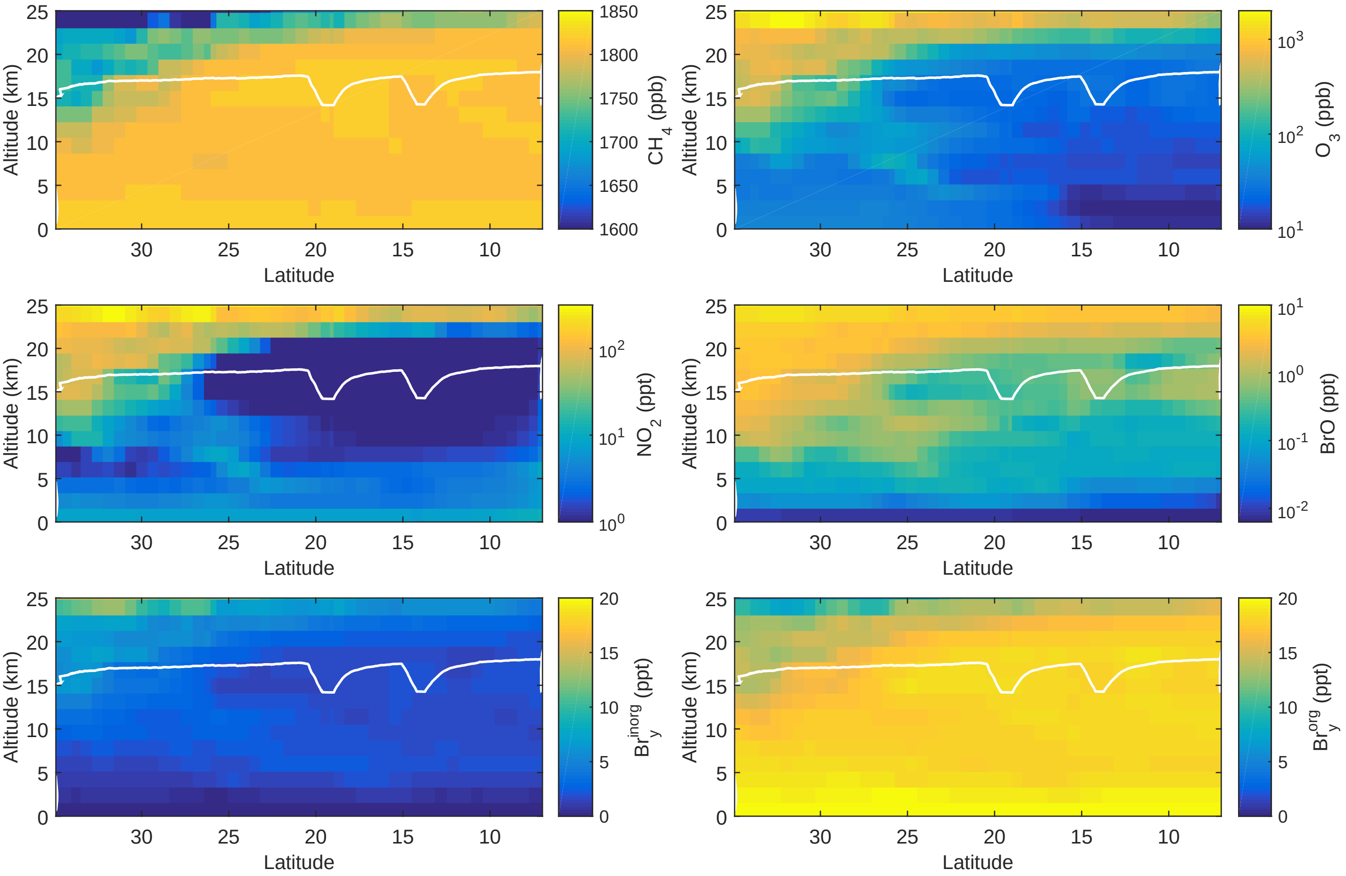

Figure 2. TOMCAT/SLIMCAT predictions of mixing ratio curtains of CH_4 (upper left), O_3 (upper right), NO_2 (middle left), BrO (middle right), Br_y^{inorg} (bottom left), and Br_y^{inorg} (bottom right) for the sunlit part of SF3-2013 (Feb. 14, 2013). Note the different color scale ranges. The white line is the flight trajectory of the Global Hawk. For better visibility, the simulated mixing ratios are shown for the altitude range 0 - 25 km, although the TOMCAT/SLIMCAT simulations cover the range of 0 - 63 km altitude

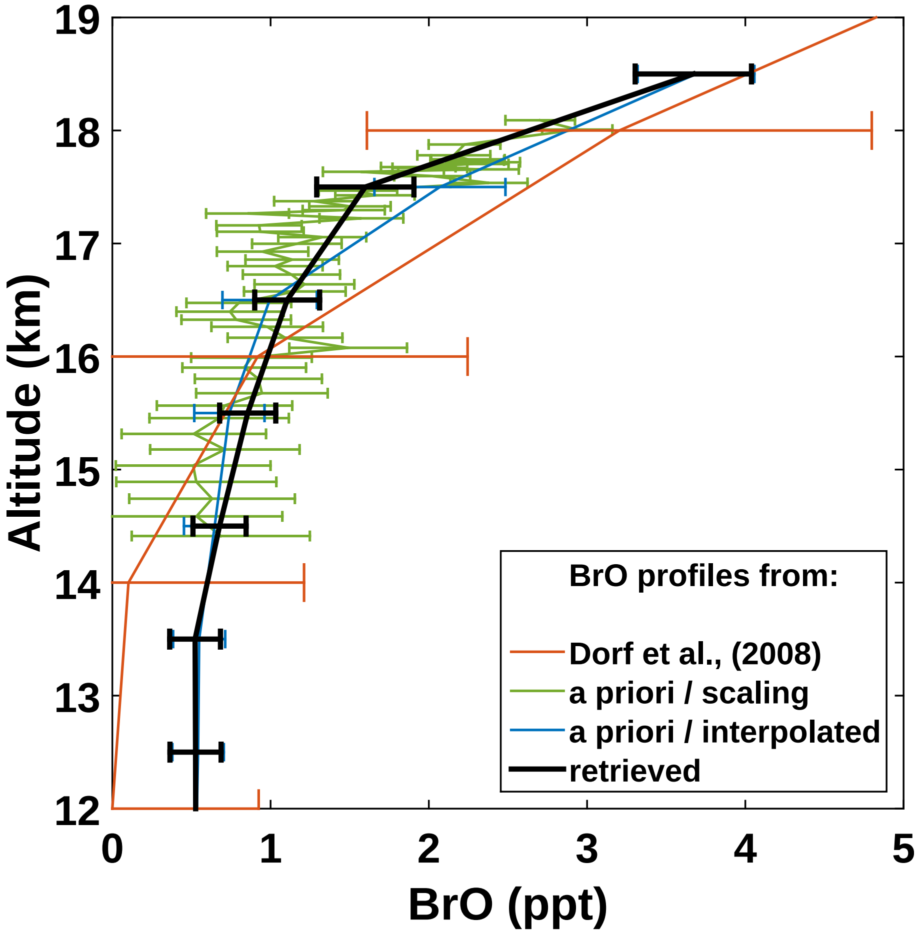

Figure 3a. Comparison of BrO profiles retrieved using the optimal estimation method (black), using the O_3-scaling technique (green), and predicted by the TOMCAT/SLIMCAT model, which is used as a priori to constrain the optimal estimation inversion retrieval (blue), and for comparison published by Dorf et al. (2008), which was measured over northeastern Brazil in June 2005 (red).

Atmos. Chem. Phys. Discuss., doi:10.5194/acp-2016-656, 2016
Manuscript under review for journal Atmos. Chem. Phys.
Published: 19 September 2016

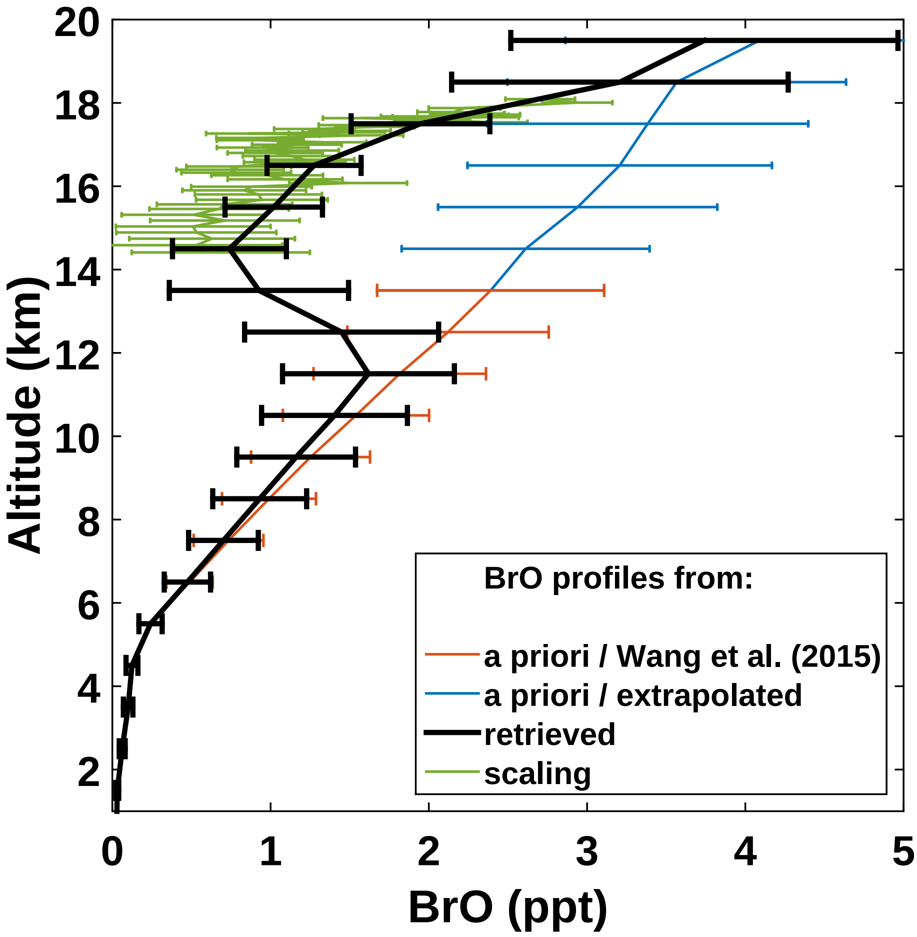

Figure 3b. Comparison of BrO profiles using the optimal estimation method (black), using the O_3-scaling technique (green), and from Wang et al. (2015) (red), which is also extrapolated to 20 km (blue). These profiles are both used as a priori in the optimal estimation. Since in the probed altitude range the inferred BrO profile (black) tend to the BrO profile obtained from the O_3-scaling technique (green), the unexpected kink around 12 to 13 km in the inferred BrO profile when the inversion is constrained to the Wang et al. (2015) BrO profile indicates that our and the Wang et al. (2015) BrO profiles are not compatible (for further details see section 4.3).

Figure 3. Comparison of the inferred BrO profiles for the ascent after dive # 2 of the flight on Feb. 5/6, 2013 with previously published (modeled and measured) BrO profiles.

Atmos. Chem. Phys. Discuss., doi:10.5194/acp-2016-656, 2016
Manuscript under review for journal Atmos. Chem. Phys.
Published: 19 September 2016

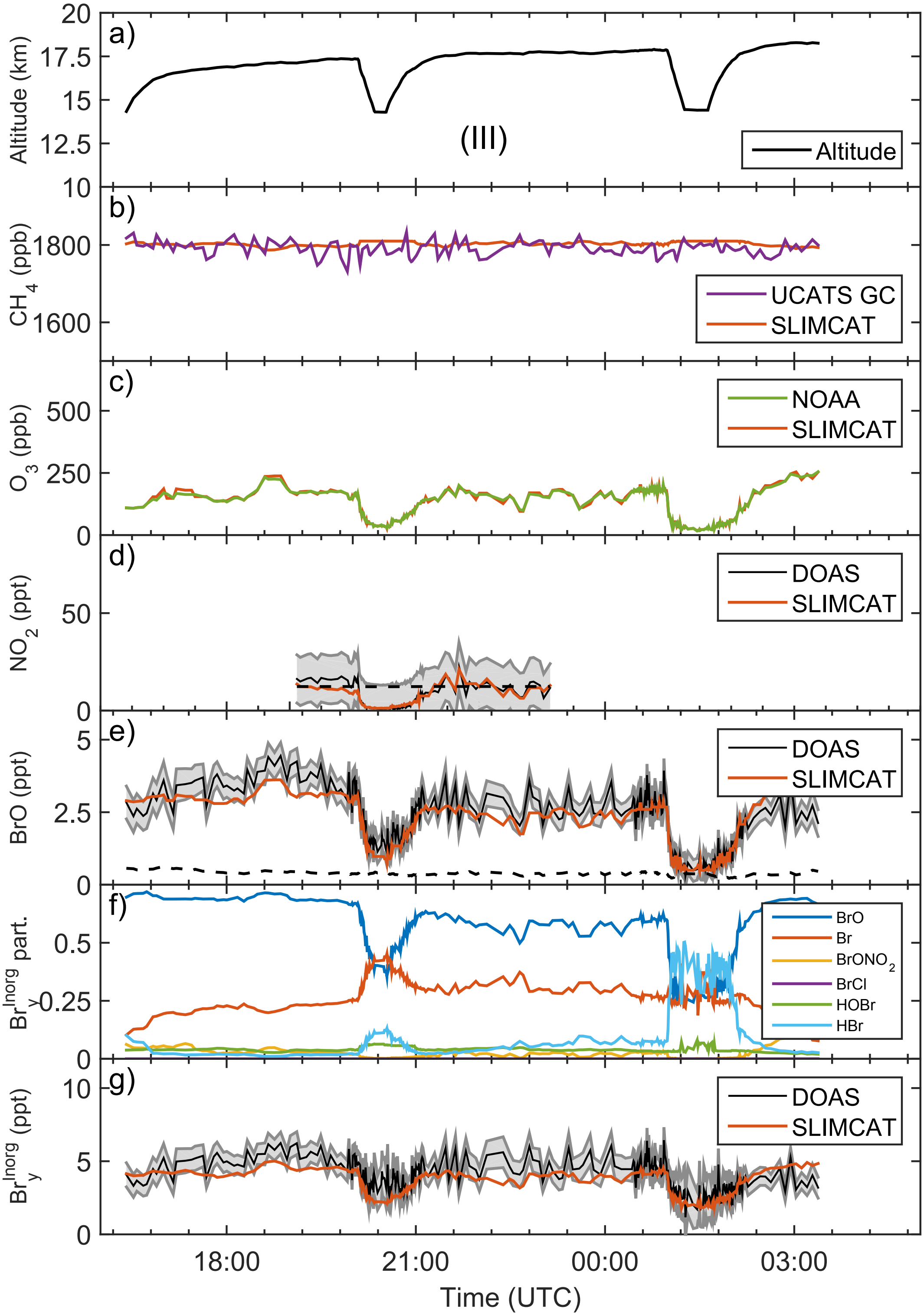

Figure 4. Panel (a) shows the time-altitude trajectory of the sunlit part of the GH flight track (SF1-2013) on Feb. 4/5, 2013 (SF1-2013). Panels (b)-(e) show intercomparisons of TOMCAT/SLIMCAT-simulated fields with observations of (b) CH_4 (UCATS), (c) O_3 (NOAA), (d) NO_2 (mini-DOAS), and (e) BrO (mini-DOAS). The grey-shaded error bars of the mini-DOAS measurements of NO_2, and BrO includes all

Atmos. Chem. Phys. Discuss., doi:10.5194/acp-2016-656, 2016
Manuscript under review for journal Atmos. Chem. Phys.
Published: 19 September 2016

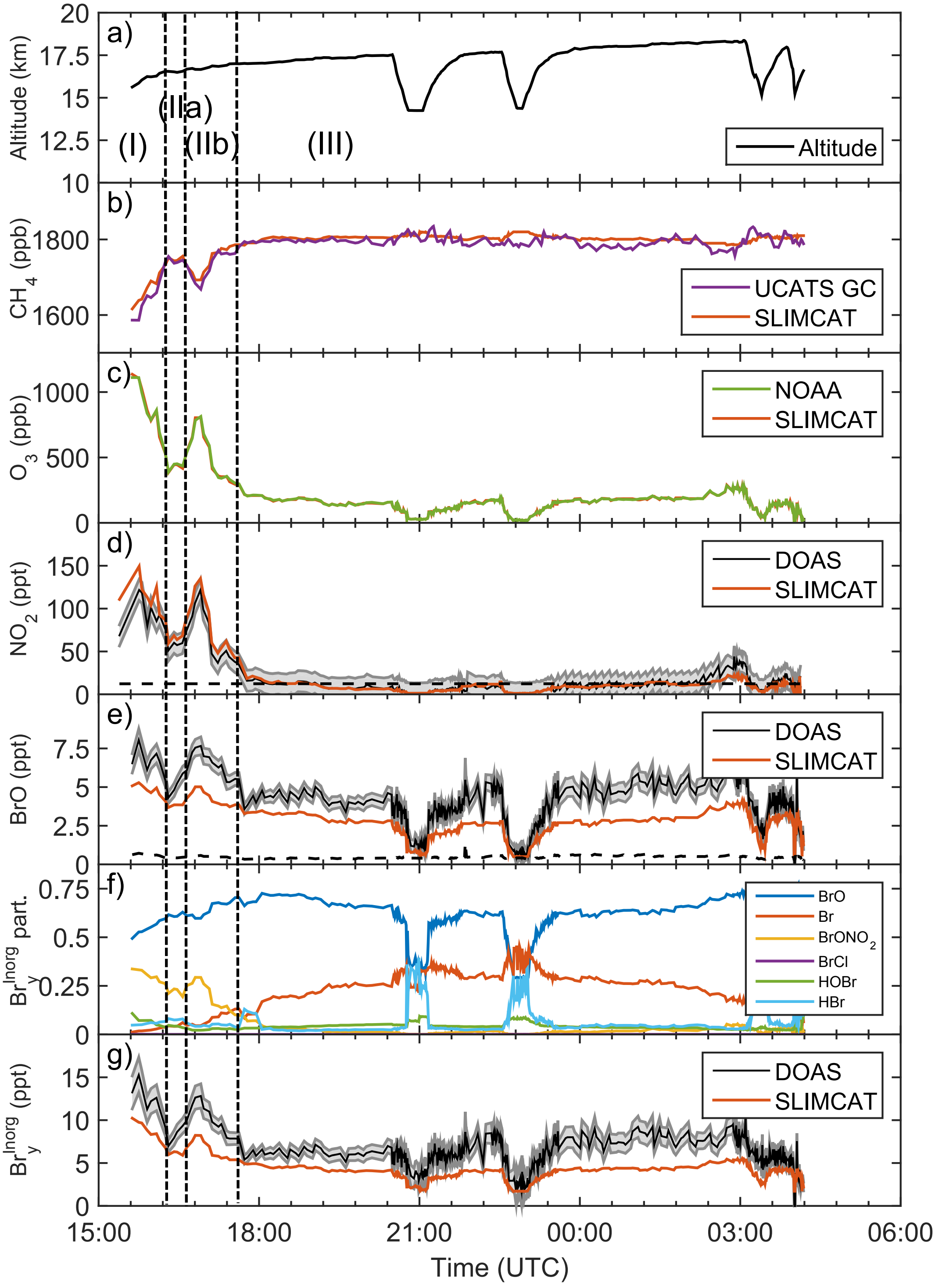

Figure 5. Same as figure 4 but for the research flight on Feb. 9/10, 2013 (SF2-2013).

Atmos. Chem. Phys. Discuss., doi:10.5194/acp-2016-656, 2016
Manuscript under review for journal Atmos. Chem. Phys.
Published: 19 September 2016

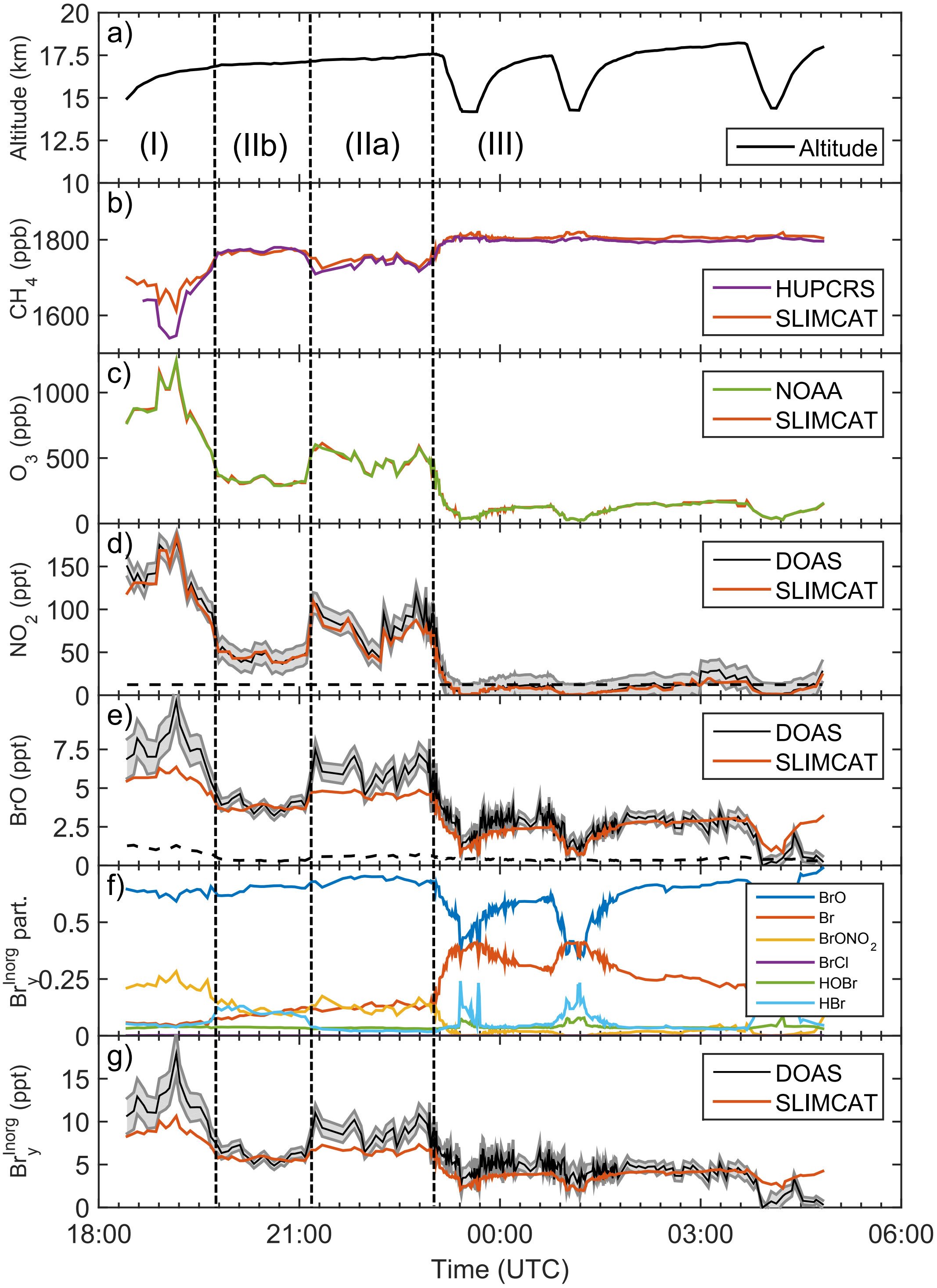

Figure 6. Same as figure 4 but for the research flight on Feb. 14/15, 2013 (SF3-2013).

Atmos. Chem. Phys. Discuss., doi:10.5194/acp-2016-656, 2016
Manuscript under review for journal Atmos. Chem. Phys.
Published: 19 September 2016

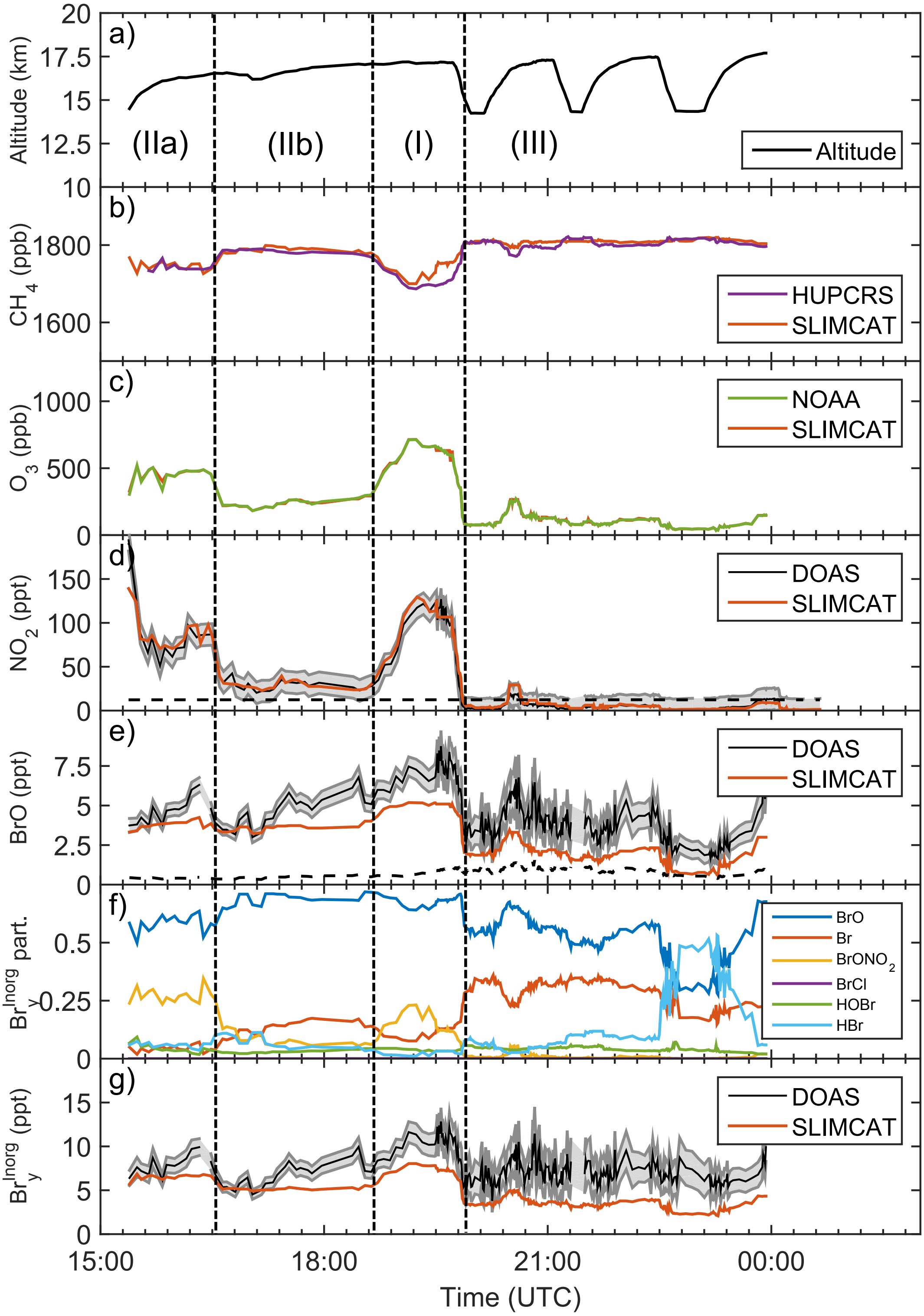

Figure 7. Same as figure 4 but for the research flight on Feb. 21/22, 2013 (SF4-2013).

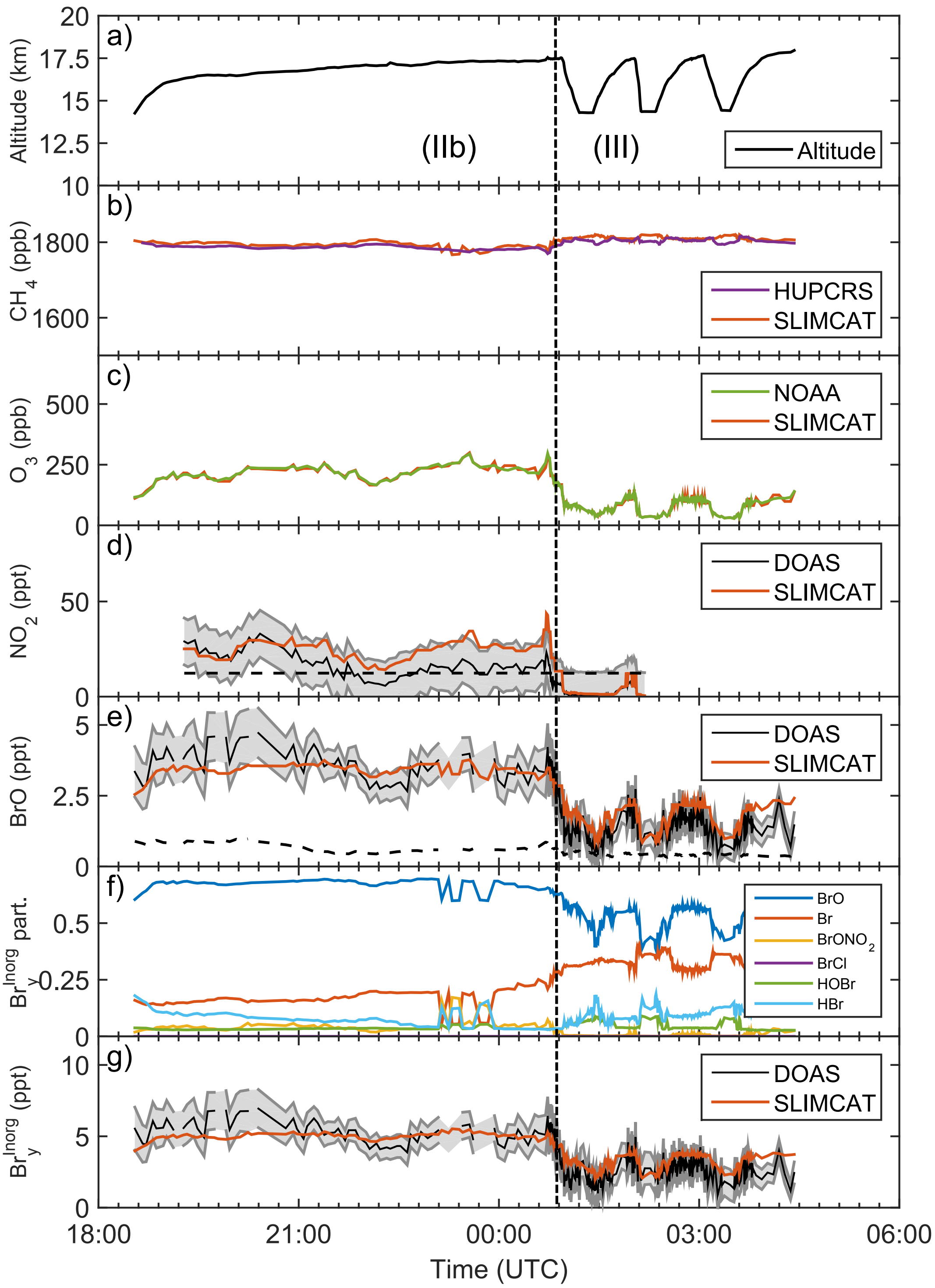

Figure 8. Same as figure 4 but for the research flight on Feb. 26/27, 2013 (SF5-2013).

Atmos. Chem. Phys. Discuss., doi:10.5194/acp-2016-656, 2016
Manuscript under review for journal Atmos. Chem. Phys.
Published: 19 September 2016

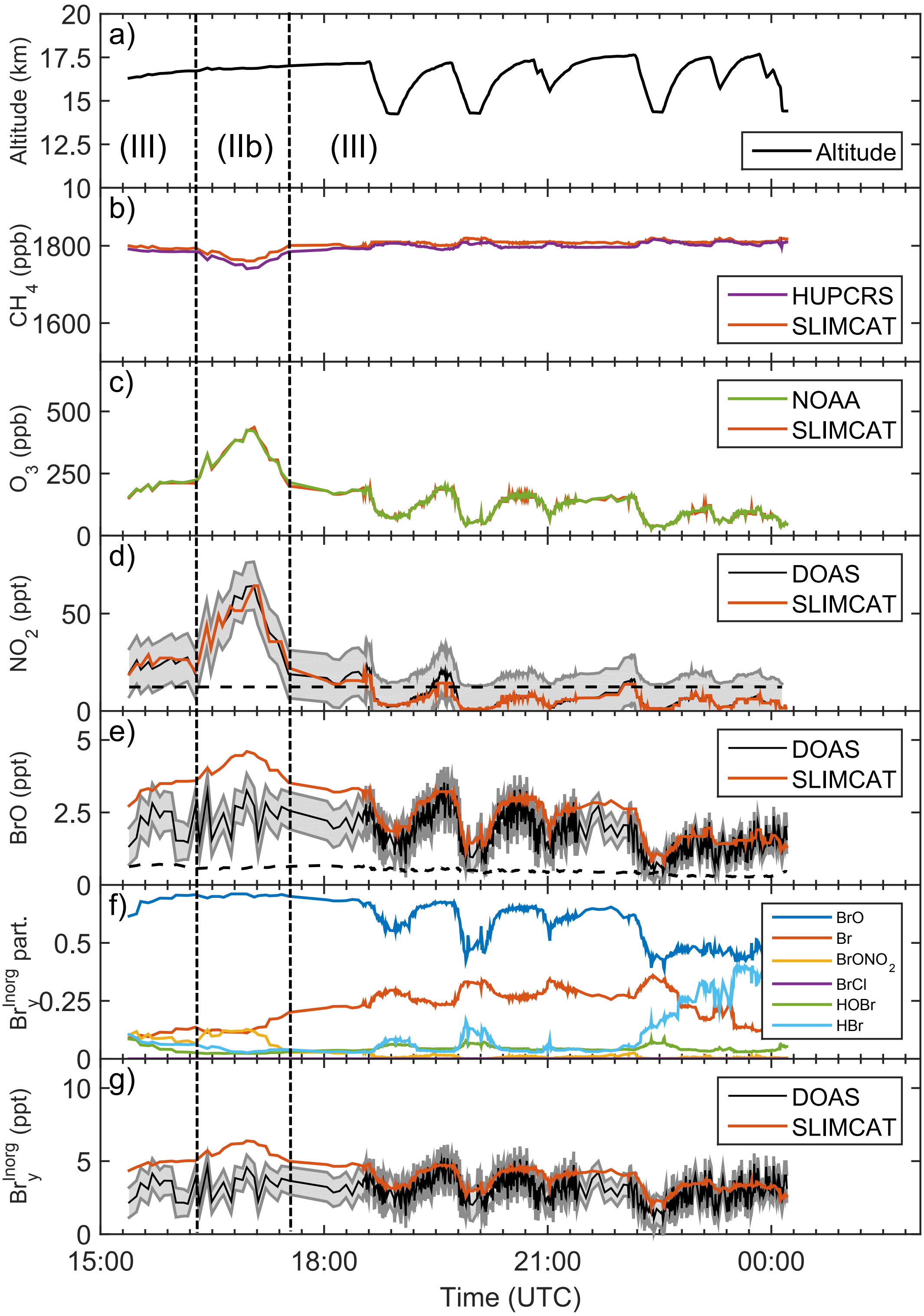

Figure 9. Same as figure 4 but for the research flight on Mar. 1/2, 2013 (SF6-2013).

Atmos. Chem. Phys. Discuss., doi:10.5194/acp-2016-656, 2016
Manuscript under review for journal Atmos. Chem. Phys.
Published: 19 September 2016

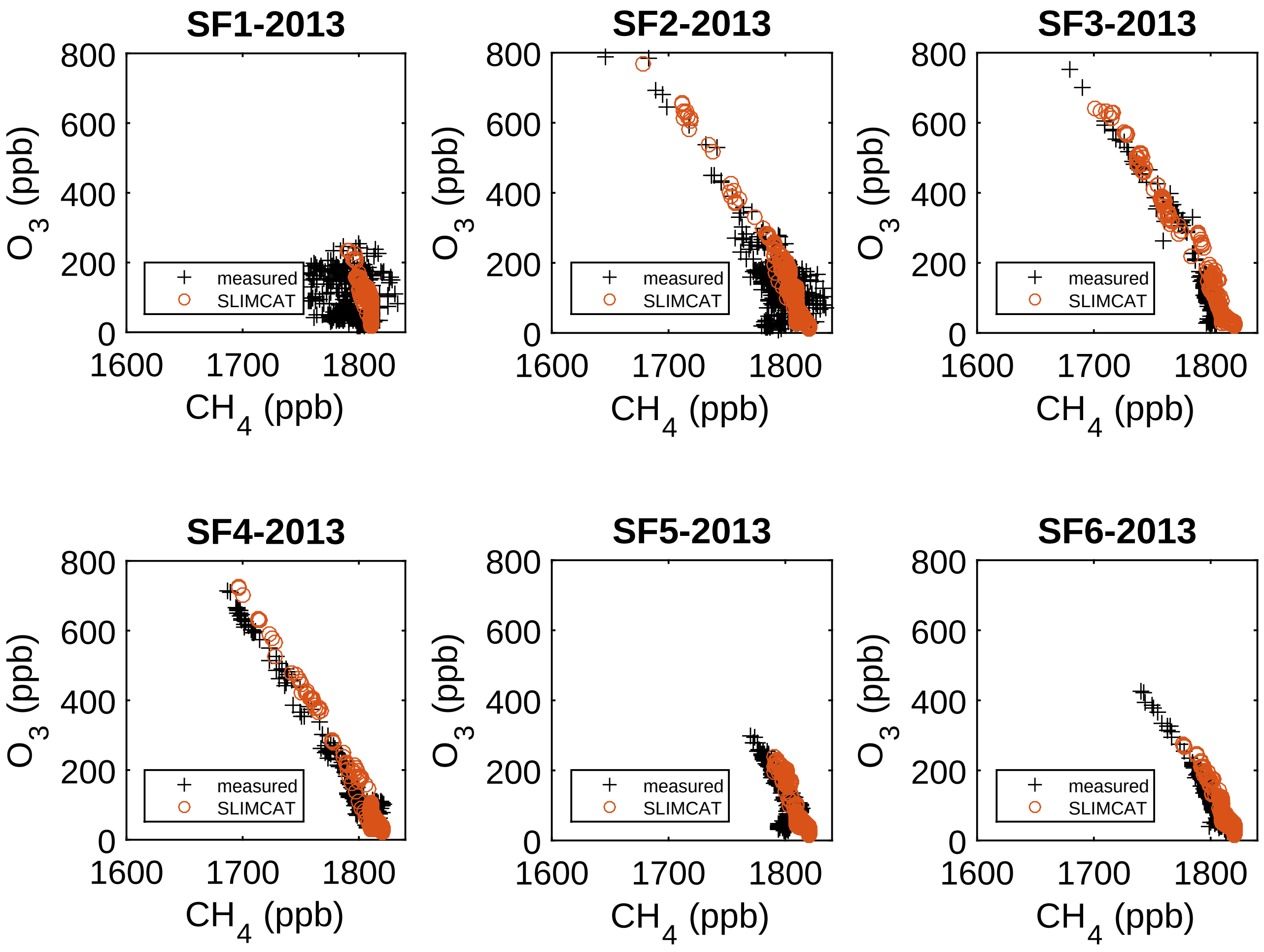

Figure 10. Correlation of observed CH_4 (UCATS SF1-2013 and SF2-2013; HUPCRS SF3-2013 to SF6-2013) and O_3 (NOAA) for the 6 NASA-ATTREX science flights in 2013. Also shown are the equivalent correlations from the TOMCAT/SLIMCAT simulation.

Atmos. Chem. Phys. Discuss., doi:10.5194/acp-2016-656, 2016
Manuscript under review for journal Atmos. Chem. Phys.
Published: 19 September 2016

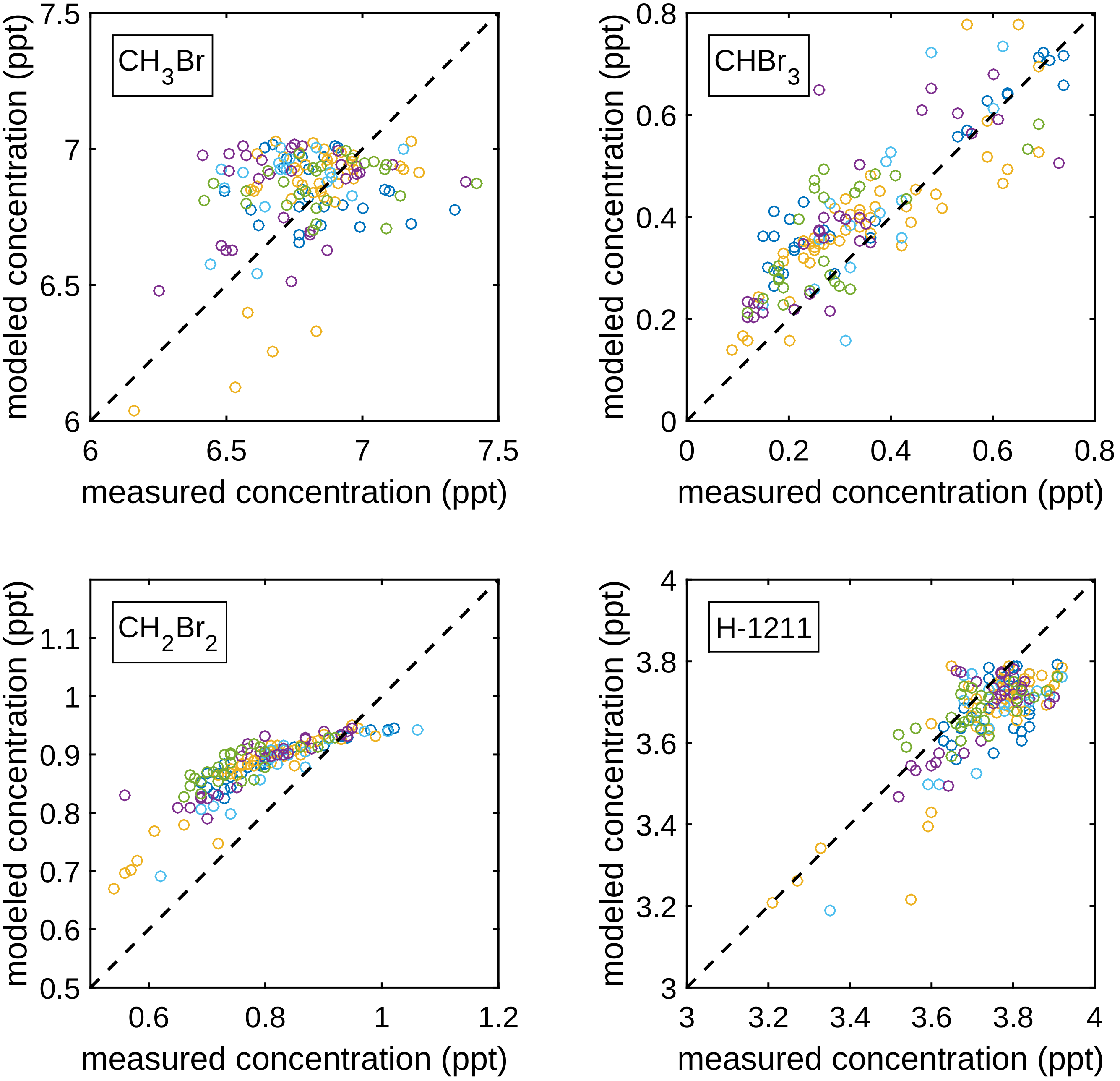

Figure 11. Correlation of GWAS measured and TOMCAT/SLIMCAT modeled major brominated source gases. Upper left panel for $CHBr_3$, upper right panel for $CHBr_3$, lower left panel for CH_2Br_2, and lower right panel for halon H1211. The concentrations for different flights are color-coded; SF1-2013 in blue, SF3-2013 in yellow, SF4-2013 light blue, SF5-2013 in purple, and SF6-2013 in green.

Atmos. Chem. Phys. Discuss., doi:10.5194/acp-2016-656, 2016
Manuscript under review for journal Atmos. Chem. Phys.
Published: 19 September 2016

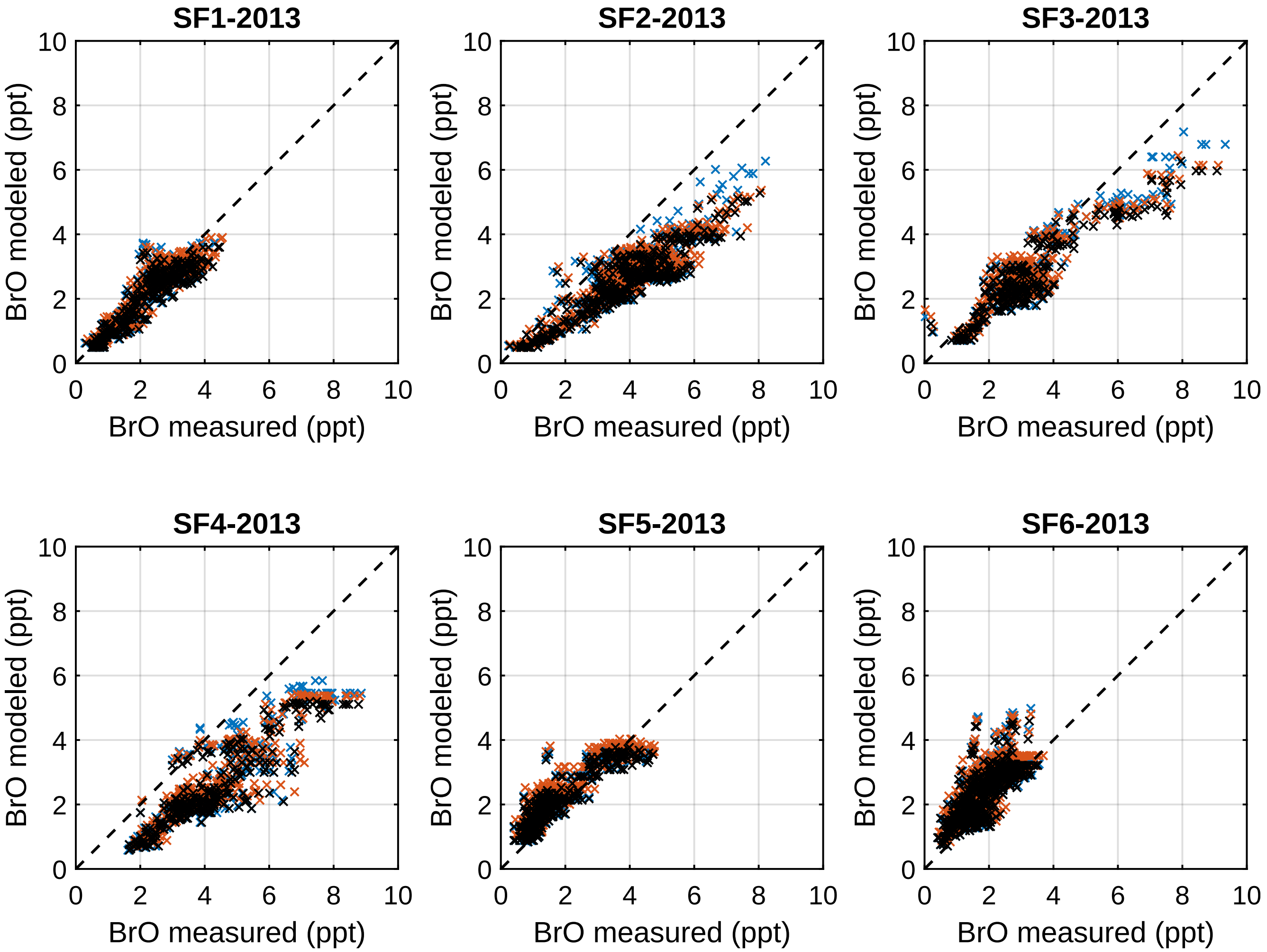

Figure 12. Comparison of measured and modeled BrO for the NASA-ATTREX science flights 1 to 6 in 2013. Black crosses are for model run # 583, blue crosses for # 584, and red crosses # 585.

Atmos. Chem. Phys. Discuss., doi:10.5194/acp-2016-656, 2016
Manuscript under review for journal Atmos. Chem. Phys.
Published: 19 September 2016

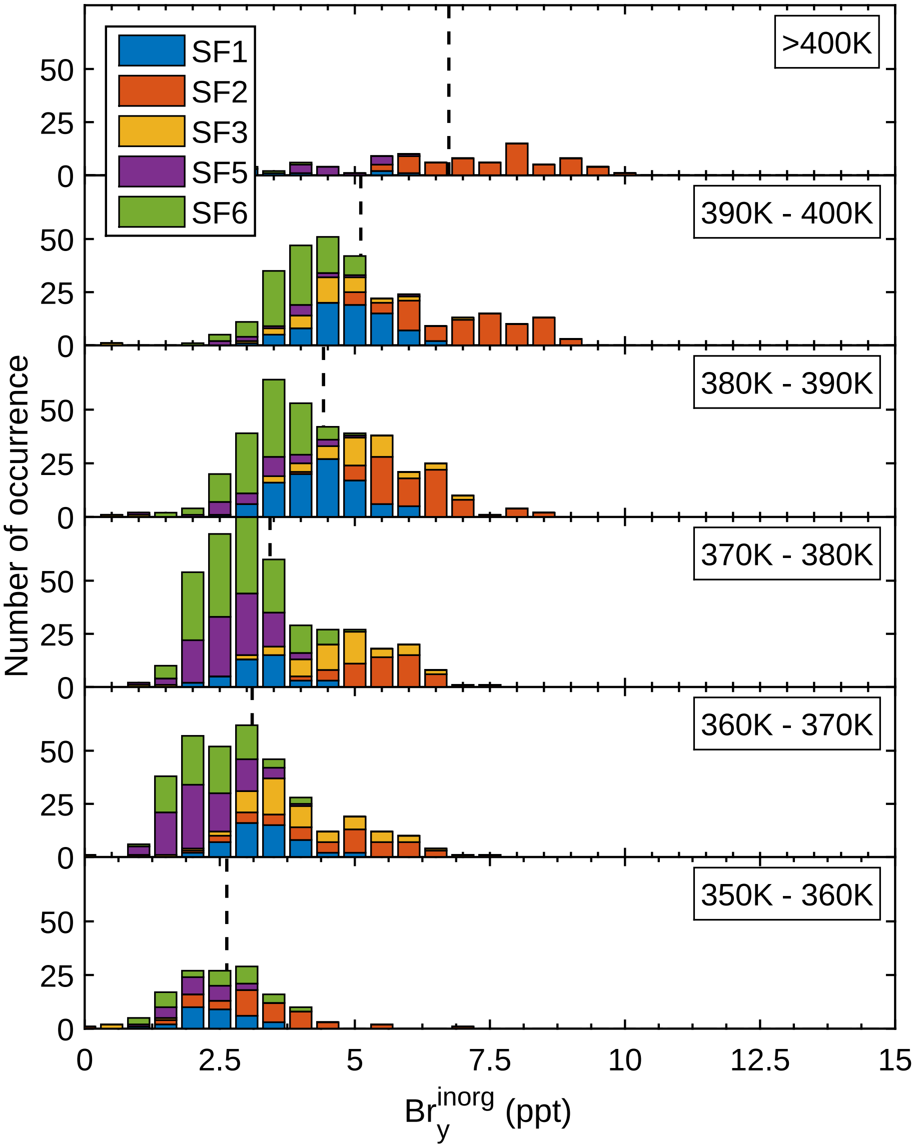

Figure 13a. Histogram of $\mathrm{Br_y^{inorg}}$ occurrence as function of potential temperature for $[\mathrm{CH_4}] \geq 1790$ ppb (as indicated in the panels), which can be considered as a marker for young air mostly found in the freshly ventilated TTL. The mean and the variance are for θ = 350 - 360 K, 2.63 ± 1.04 ppt; θ = 360 - 370 K, 3.1 ± 1.28 ppt; θ = 370 - 380 K, 3.43 ± 1.25 ppt; θ = 380 - 390 K, 4.42 ± 1.35 ppt; θ = 390 - 400 K, 5.1 ± 1.57 ppt, and $\theta \geq$ 400 K, 6.74 ± 1.79 ppt, respectively.

Atmos. Chem. Phys. Discuss., doi:10.5194/acp-2016-656, 2016
Manuscript under review for journal Atmos. Chem. Phys.
Published: 19 September 2016

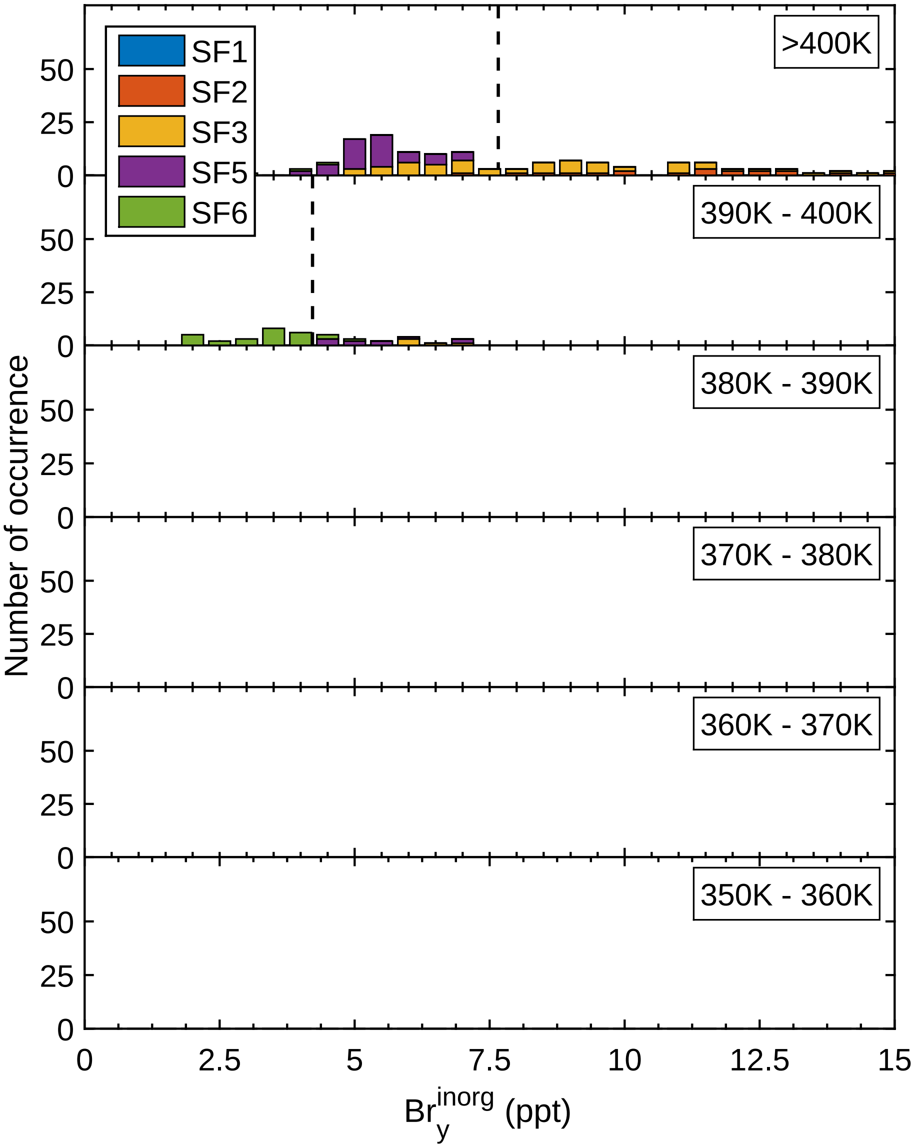

Figure 13b. Histogram of Br_y^{inorg} occurrence as function of potential temperature for $[CH_4] \leq 1790$ ppb, which can be considered as a marker for aged air mostly found in the subtropical lowermost stratosphere. The mean and the variance are for θ = 390 - 400 K, 4.22 ± 1.37 ppt, and $\theta \geq 400$ K, 7.67 ± 2.72 ppt, respectively.

Figure 13. Histogram of Br_y^{inorg} occurrence as function of potential temperature for all NASA-ATTREX flights in 2013. The dashed lines mark the mean Br_y^{inorg} concentration for each potential temperature range.

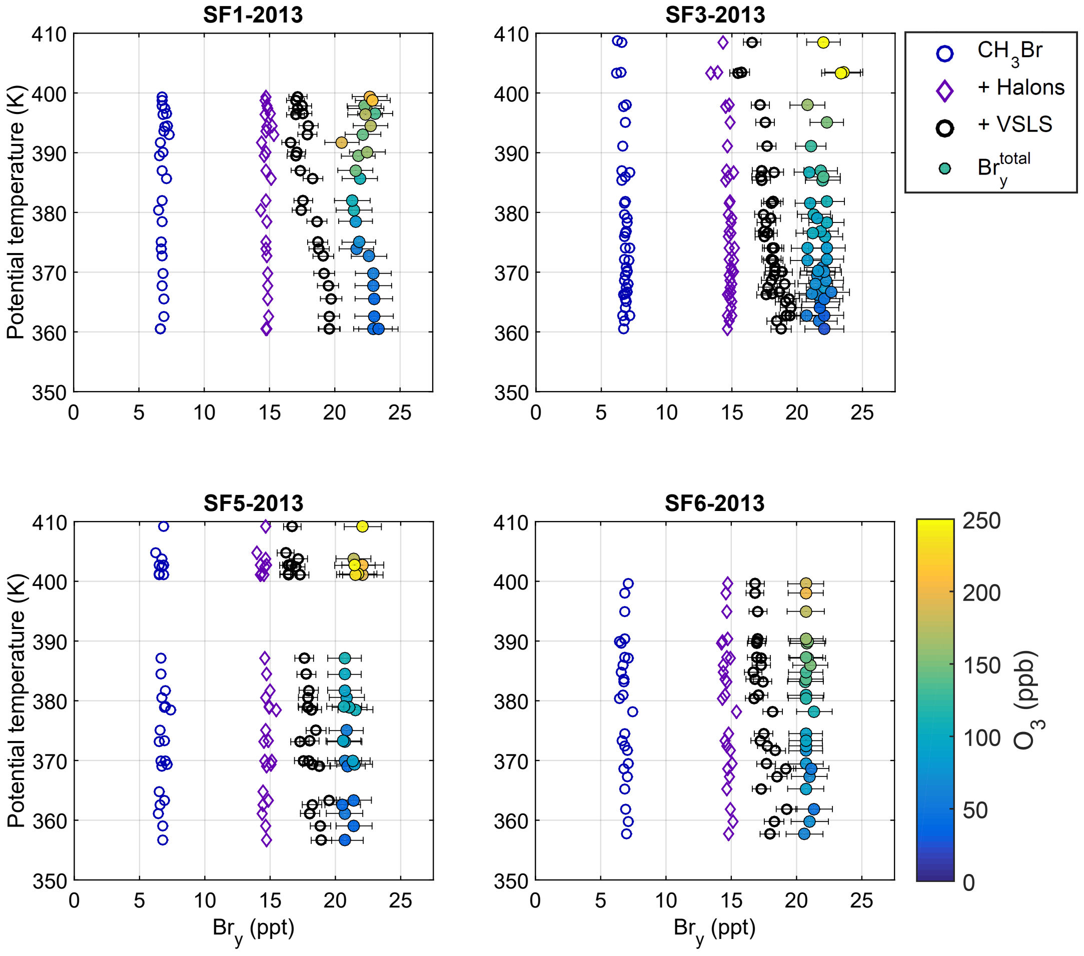

Figure 14. Br_y as a function of potential temperature (θ) for all dives during the 2013 NASA-ATTREX flights, when joint measurements of Br_y^{org} and Br_y^{inorg} are available.

Atmos. Chem. Phys. Discuss., doi:10.5194/acp-2016-656, 2016
Manuscript under review for journal Atmos. Chem. Phys.
Published: 19 September 2016

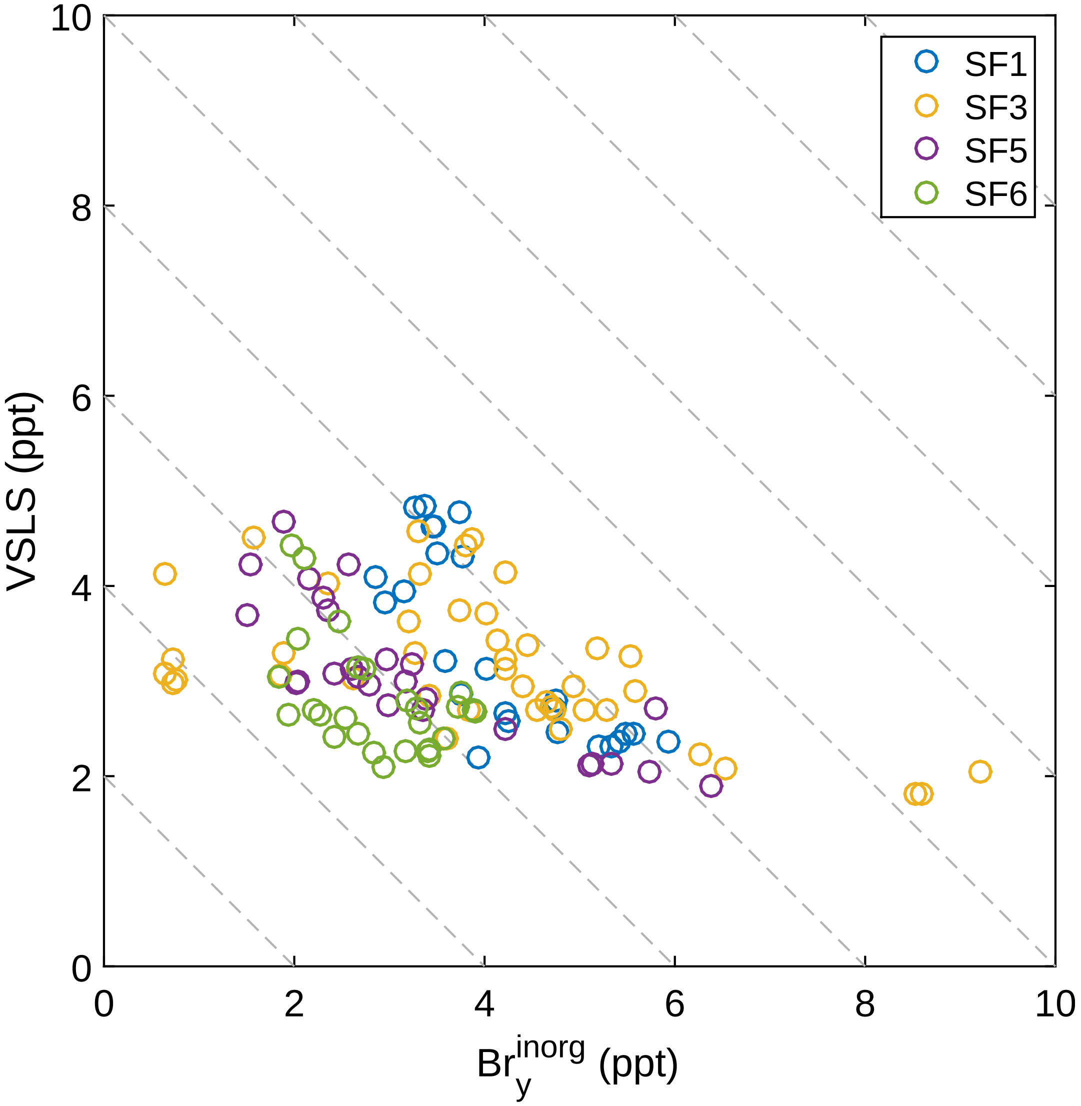

Figure 15. Br_y^{inorg} as a function of the sum of all brominated VSLS using the same color code as in figure 11. If all Br_y^{inorg} was produced from the same air masses with the same amount of brominated organic VSLS concentrations available at the surface, all data points should follow individual diagonal lines.